Revision 1

Word Count: 8050

Raman spectroscopy-based screening of zircon for reliable water content and oxygen isotope measurements

Chuan-Mao Yang[a, b, c], Yi-Gang Xu[a, b, d*], Xiao-Ping Xia[a, b*], Yu-Ya Gao[e, f], Wan-Feng Zhang[a, b], Ya-Nan Yang[a, b], Qing Yang[a, b], Le Zhang[a, b]

[a] *State Key Laboratory of Isotope Geochemistry, Guangzhou Institute of Geochemistry, Chinese Academy of Sciences, Guangzhou 510640, China*

[b] *CAS Center for Excellence in Deep Earth Science, Guangzhou, 510640, China*

[c] *College of Earth and Planetary Sciences, University of the Chinese Academy of Sciences, Beijing 100049, China*

[d] *Southern Marine Science and Enginerring Guangdong Laboratory (Guangzhou), 511458, China*

[e] *Institute of Geology and Geophysics, Chinese Academy of Sciences, Beijing 100029, China*

[f] *National Institute of Metrology, Beijing 102200, China*

Abstract

Water content and oxygen isotopes in zircon provide crucial constraints on magma source and process, yet they can be significantly modified by zircon metamictization, which causes secondary water absorption into the zircon crystal and the concomitant oxygen isotope changes. Therefore, it is imperative to develop a screening scheme to select the least-metamict zircons for the analyses. We propose a screening scheme based on our study on the Suzhou A-type granite (South China), through integrating zircon laser Raman spectroscopy, water and trace element contents, and oxygen isotopes. The results show that the primary water content is retained in zircon when the Full Width at Half Maximum (FWHM) is <8 cm^{-1} or the Raman shift is >1007 cm^{-1} of $\nu_3(SiO_4)$ vibration band, whilst the primary $\delta^{18}O$ is preserved at <10 cm^{-1} FWHM or >1005.5 cm^{-1} Raman shift. Changes of trace element concentrations in Suzhou zircons are different from previous observation in metamict zircons but most likely related to magma evolution, which implies trace elements are insensitive to metamictization. Primary $\delta^{18}O$ in Suzhou zircons (4.5-6.0‰) fall into the mantle range, indicating a dominant mantle contribution to Suzhou granites. Primary water content was estimated at ca. 650–1400 ppm, significantly higher than that in typical I-type granites (400-736 ppm) and the upper mantle-derived zircons (81-177 ppm). The high primary zircon water content was not controlled by sub-solidus process, temperature, pressure and cation charge balance but considered to reflect the high-water content in melts. This suggests a hydrous origin for the Suzhou A-type granite, which challenge the conventional view of anhydrous petrogenesis for A-type granites.

Keyword: Zircon water content; A-type granite; Laser Raman spectroscopy; Full Width at Half Maximum (FWHM); Raman shift; SIMS; Trace element

Introduction

Zircon is a ubiquitous uranium-rich accessory mineral in magmatic rocks, characterized by high physical and chemical stability (Valley et al., 1998; Wilde et al., 2001). The abundant U-Th and low common Pb contents make zircon the most important mineral in geochronology (Davis et al., 2003). Meanwhile, trace elements in zircon are very useful in evaluating the magma properties (Bell et al., 2017; Burnham and Berry, 2012; Fu et al., 2008; Griffin et al., 2002; Trail et al., 2012; Valley et al., 1994; Watson et al., 2006; Zou et al., 2019). For example, Ti-in-zircon thermometry has been widely used to estimate the magma temperature (Fu et al., 2008; Watson et al., 2006), and the zircon Eu and Ce anomalies of intermediate-felsic rocks are sensitive proxies for crustal thickness (Tang et al., 2020, 2021) and magma oxygen fugacity (Burnham and Berry, 2012; Trail et al., 2012; Zou et al., 2019), respectively. In addition, zircon Hf-O isotopes have been well demonstrated to be useful tracer of magma source and processes (Griffin et al., 2002; Kemp et al., 2007; Valley et al., 1994).

Over the past decades, numerous investigations have been carried out to estimate the water contents in zircon (Aines and Rossman, 1986; Caruba et al., 1985; De Hoog et al., 2014; Ingrin and Zhang, 2016; Pidgeon et al., 2013; Trail et al., 2010; Wang et al., 2018; Woodhead et al., 1991b; Xia et al., 2019; Zhang et al., 2010; Zhang, 2015). It is suggested that the diffusion coefficient of water in zircon is 1 to 2 orders of magnitude lower than in other nominally anhydrous minerals (NAMs), e.g., olivine, orthopyroxene and garnet (Ingrin and Zhang, 2016; Zhang, 2015). This means that

72 water has a higher closure temperature in zircon, and that the primary water could be
73 well preserved in zircon (Ingrin and Zhang, 2016; Zhang, 2015). Given the pivotal
74 influence of water on magmatic processes (Campbell and Taylor, 1983; Clemens et al.,
75 2020; Collins et al., 2020; Johannes and Holtz, 2012), such as partial melting and
76 fractionation, study of zircon water content would also yield new insights into these
77 processes.

78 As a NAM, zircon hosts water mainly in the form of OH in its defect structure
79 (Caruba et al., 1985; Nasdala et al., 2001a; Woodhead et al., 1991b). Trace amount of
80 water that partitions into zircon from the melt during its crystallization is termed
81 primary water here, which can be used to infer the water content in the melt (De Hoog
82 et al., 2014; Trail et al., 2010). The assignment of primary water is not straightforward
83 because secondary water can enter zircon as OH or H_2O molecules after the magma
84 solidified (Aines and Rossman, 1986; Breiter et al., 2014; Nasdala et al., 2001a, 2009;
85 Pidgeon et al., 2013; Woodhead et al., 1991a, b; Zhang et al., 2010), thus interfering
86 with the amount of true primary water in the melt and altering the zircon oxygen
87 isotope compositions (Gao et al., 2014; Pidgeon, 2014; Wang et al., 2014).

88 Secondary water in zircon may have resulted from the structural damage through
89 α-decay of U and Th (Aines and Rossman, 1986; Breiter et al., 2014; Nasdala et al.,
90 2009; Pidgeon et al., 2013; Woodhead et al., 1991a, b). Accumulation of radiation
91 damage leads to zircon metamictization through expansion of crystal lattice and
92 decrease of chemical stability of zircon, which would markedly increase the water
93 storage capacity (Aines and Rossman, 1986; Ewing et al., 2003; Nasdala et al., 2001a;

Woodhead et al., 1991a). As revealed by infrared spectroscopy, the primary water content of zircon is generally about 0.01 wt% (Woodhead et al., 1991a), but secondary water in metamict zircon could reach up to 16.3 wt% (Aines and Rossman, 1986). Therefore, it is crucial to determine the degree of zircon metamictization and select the least metamict zircons for obtaining reliable primary water content and oxygen isotope compositions.

The degree of zircon metamictization can be quantified by the radiation dose D_{dpa}, calculating which would require the U and Th contents and age of zircon (Ewing et al., 2003). Moreover, healing of radiation damage in annealed zircons would often lead to overestimation of the actual degree of metamictization (Pidgeon, 2014). The expand crystal lattice often accommodate more incompatible trace elements in zircons. Thus, the incompatible element concentration in zircons could be regarded as indicators of metamictization (Belousova et al., 2002; Horie et al., 2006). However, this method would no longer work when outside would not supply enough incompatible elements. Laser Raman spectroscopy, which has the advantages of being non-invasive and easy-to-use, can be used to measure the degree of zircon metamictization (Geisler et al., 2001; Nasdala et al., 1995, 2001a; Zhang et al., 2000). This is because Raman spectra change systematically with increasing degree of actual metamictization. Crystalline zircon shows unique sharp internal and external vibration peaks in the 200–1010 cm^{-1} spectral range (Nasdala et al., 1995, 2001b). As the degree of radiation damage increases, the main band intensity of the Raman spectrum decreases, with broader width and distinct shift to lower wave number (Nasdala et al., 1995, 2001b).

The short-range order decrease in radiation-damaged zircon is caused by the large amount of irregularly-located atoms and the bond-lengths/-angles produced by the U and Th nuclear fission (Ewing et al., 2003). The width of antisymmetric stretching vibration mode of Si-O tetrahedron, i.e., $\nu_3(SiO_4)$, and the wave number (1010 cm^{-1} in crystalline zircon) determine the degree of short-range order around the position of four-fold coordinated Si atoms (Nasdala et al., 1995, 2001b). This band is the most sensitive in characterizing the degree of zircon metamictization (Nasdala et al., 1995, 2001b). The Full Width at Half Maximum (FWHM) of this band is <3 cm^{-1} and >30 cm^{-1} for high-crystallinity zircon and highly-metamict zircon, respectively (Nasdala et al., 2001b).

Although many Raman spectroscopy-based quantitative screening criteria for the degree of zircon metamictization have been proposed, none are tailored for water content and oxygen isotope analyses. Zircons from the Suzhou granite (Jiangsu province, South China) are selected in this study due to their wide ranges of metamictization intensity, and U (33–13,433 ppm) and Th (23–17,028 ppm) contents (Gao et al., 2014). The minimum natural "fading" or annealing of radiation damage in these zircons also make them suitable to test the screening criteria (Gao et al., 2014). In this paper, we present Raman spectroscopy, in situ oxygen isotopes, water contents and trace element measurements for zircon grains of the Suzhou A-type granites. Based on the relations between zircon water content/oxygen isotope and Raman spectroscopic parameters, we propose FWHM <8 cm^{-1} or Raman shift >1007 cm^{-1} as the screening criteria for water content of the least-metamict zircons. We also found

that the primary water content in our zircon samples is surprisingly high, which challenges the current view on the anhydrous origin of A-type granites.

Sample descriptions

The Early Cretaceous Suzhou A-type granites are geologically located at the junction between the Dabie-Lower Yangtze Reach magmatic belt and the coastal magmatic belts in south-eastern China. The batholith is located 8 km west of the Suzhou City, with an outcrop of about 50 km^2 (Charoy and Raimbault, 1994; Gao et al., 2014; Wang et al., 1993; Wang et al., 1996; Wei et al., 2008). The granites are mainly composed of K-feldspar (~60 vol%), quartz (~30 vol%), and interstitial biotite (<5 vol%) and hornblende (<3 vol%; Gao et al., 2014). Most feldspars developed trans-/hyper-solvus texture, and hydrothermal alteration and weathering were developed along the pluton margin (Gao et al., 2014). The Suzhou granites are rich in REEs, HFSEs, U, and Th, and are regarded as typical "low $\delta^{18}O$" (4.66–5.13‰) A-type granites in Eastern China (Wei et al., 2008). Previous studies concluded that the granites are volatile-rich (e.g., F) but water-deficient (Charoy and Raimbault, 1994).

Based on petrography and isotopic age (Chen et al., 1993; Ouyang, 1985; Wang et al., 1993), the Suzhou granite batholith has been considered to be an intrusive complex with three magmatic phases: (from oldest to youngest) (1) porphyritic amphibole-bearing alkali-feldspar granite, (2) coarse-grained alkali-feldspar granite (dominant, ~70% of the total outcrop), and (3) fine-grained alkali-feldspar granite (Charoy and Raimbault, 1994; Wang et al., 1996). The crystal caves, mainly

distributed on the top and edge of the plutons, are observed in all three phases and are most developed in the coarse-grained granite (Wang et al., 1993). Further studies acquired refined zircon U-Pb ages that all of three-phase granites have an identical age within the error with an average age of 126.1 ± 0.5 Ma, indicating they were formed in a single magmatic event (Gao et al., 2014).

Four zircon samples (Sz1, Sz2, Sz3, Sz4) from the three granite phases (Gao et al., 2014) were analyzed in this study. The zircon grains are 50–200 μm long and mostly euhedral-subhedral, with aspect ratios of 1:1 to 1:3 (Fig. 1). Fluid and mineral inclusions are common in these zircons, and the zircons in phase-2 granite (Sz2 and Sz4) are finer than those from phase-1/-3 granite (Sz1 and Sz3) (Fig. 1; Chen et al., 1993; Gao et al., 2014). Gao et al. (2014) divided the zircons into two groups: Group 1 zircons have clear oscillatory zoning and high cathodoluminescence (CL) reflectance (Fig. 1), whilst Group 2 zircons are brown, and have low CL reflectance and no discernible oscillatory zoning (Fig. 1), indicating high U-Th contents and intense metamictization. Phase-3 fine grained granite contains abundant dark zircon grains, which is revealed in the sample Sz3 (Fig. 1). Cracks are common in the zircon samples, many of which contain distinct corrosion pits as well (Fig. 1; Gao et al., 2014), probably reflecting partial dissolution during alteration (Gao et al., 2014).

Analytical methods

All the zircon sample grains and the in-house zircon standards of Qinghu and Penglai were mounted on Sn-based alloy following the method of Zhang et al. (2018),

and then polished down to expose half of the crystals. All zircon grains were observed under reflected-light micrography and CL imaging to reveal their internal texture. With these images, the domains free of inclusions, fractures, or surface contamination are chosen for further analyses.

Laser Raman spectroscopy

Laser Raman analysis was performed with a Renishaw 2000 Raman spectrometer at the Guangzhou Institute of Geochemistry, Chinese Academy of Sciences (GIGCAS). The data acquisition program parameters have been carefully standardized to obtain reliable radiation damage information. The laser Raman spectral light source is a 532 nm argon laser, the telephoto objective lens has a 20X magnification, with 1 cm^{-1} resolution, and 3 μm×3 μm spot size. The Raman signal generated by the samples is split by an 1800 l/mm grating, and then collected by a thermoelectric cooled CCD. The time of spectral collection varies according to the signal intensity (10–200 s). 100–1800 cm^{-1} full-wavelength spectrum was taken at one time, and the single crystal silicon wafer was used to calibrate the Raman spectra before the measurement. The Raman shift of the single crystal silicon wafer was corrected to corresponding to 520.7 cm^{-1}. The Raman spectral background can be strongly affected by the laser-induced fluorescence of rare earth elements (REEs) (Gaft et al., 2000), and hence baseline calibration needs to be performed for every individual grain. Here, we used a cubic polynomial to fit the spectral data, which are less affected by the zircon vibration peaks to acquire the baseline. The FWHM of Gaussian function that fitted to $\nu_3(SiO_4)$ vibration band was taken as the FWHM of

206 $\nu_3(SiO_4)$ band.

207 **Zircon oxygen isotope and water content measurement**

208 The zircon oxygen isotope and water content were measured simultaneously with a
209 Secondary Ion Mass Spectrometry (SIMS, CAMECA IMS 1280-HR) at GIGCAS.
210 The analyzed domains of SIMS are exactly the same as those of the Raman
211 spectroscopy. After vacuum-coated by ~30 nm-thick gold film, the mount was loaded
212 into the storage chamber overnight. Before the analysis, the mount was further
213 pumped down in the analysis chamber, and the vacuum of the analysis chamber could
214 reach 1.9×10^{-9} mbar. A Cs^+ source of 3–5 nA with 10 kV impact energy was set to
215 sputter secondary ions. The area (50×50 μm) was sputtered before the analyses to
216 remove the coating and reduce surface contamination, and the size of the analytical
217 area was about 30×30 μm (15 μm spot size + 15 μm rastering). Two Faraday cup
218 detectors (10^{10} Ω and 10^{11} Ω resistance) were used to detect ^{16}O and ^{18}O ions, and an
219 electron multiplier was used to measure $^{16}O^{1}H$ at same time. For ^{16}O and ^{18}O, a 500
220 μm collector slits were used to generate ~2500 MRP. For $^{16}O^{1}H$, a 173 μm collection
221 slit (corresponding to ~7000 MRP) was used to avoid ^{17}O interference.

222 Under such conditions, ^{16}O ion yield of ~4×10^{8} counts/s·nA was detected. A single
223 spot analysis lasted for 4.5 minutes, including 200 s pre-analysis and secondary ion
224 beam automatic centering, and ~1 minute to integrate 20 cycles of static measurement
225 of $^{16}O^{1}H$, ^{16}O and ^{18}O. The internal precision of $^{18}O/^{16}O$ and $^{16}O^{1}H/^{16}O$ are usually
226 better than 0.4‰ and 0.5% (2SE). The measured $^{16}O^{1}H/^{16}O$ was converted to zircon
227 water content according to the calibration curve constructed by measuring a set of

zircon reference samples (Xia et al., 2019; Zhang et al., 2020). The measurement limitation of water content is ~10 ppm and uncertainty of the calibrated water content is ~10% (Xia et al., 2019). The $^{18}O/^{16}O$ value was normalized to the Vienna Standard Mean Ocean Water (VSMOW: $^{18}O/^{16}O$ = 0.0020052). The instrumental mass fractionation of oxygen isotopes was calibrated with the Penglai zircon standard ($\delta^{18}O$ = 5.3‰; Li et al., 2010).

In situ trace element analyses

Trace elements in zircons were measured with an ELEMENT XR inductively coupled plasma-mass spectrometer (ICP-MS) coupled with a 193-nm (ArF) Resonetics RESOlution M-50 laser ablation system at the GIGCAS. Laser ablation conditions include 33 μm beam size, 5 Hz repetition rate, and 4 J cm^{-2} energy density. A smoothing device (the Squid, Laurin Technic) was used to smoothen the sample signal. Each spot analysis consisted of 20 s laser-off gas blank collection, and 30 s laser-on sample signal detection. Measurement was conducted under the E-scan mode. Signals of the following masses were detected: ^{27}Al, ^{29}Si, ^{31}P, ^{45}Sc, ^{47}Ti, ^{89}Y, ^{93}Nb, ^{139}La, ^{140}Ce, ^{141}Pr, ^{146}Nd, ^{147}Sm, ^{151}Eu, ^{157}Gd, ^{159}Tb, ^{162}Dy, ^{165}Ho, ^{166}Er, ^{169}Tm, ^{174}Yb, ^{175}Lu, ^{178}Hf, ^{232}Th and ^{238}U. NIST610 was used as the external calibration standard. The oxide molecular yield, indicated by the $^{238}U^{16}O/^{238}U$ ratio, was below 0.3%. Detailed experiment procedure and data reduction strategy were as described by Zhang et al. (2019). NIST612 was measured as unknown samples. 30 analyses of NIST612 indicate that the contents of most elements are within 8% of the reference values, and that the analytical precision (2 RSD) was better than 10% for most elements.

250

251 # Results

252 ## Laser Raman spectroscopy

253 The Raman spectra of 129 zircon grains (from four samples) were collected. The
254 Raman spectra baseline corrected results of typical highly-metamict (Sz2@01) and
255 pristine crystalline (Sz3@04) zircons are shown in Figures 2a and 2b. The
256 fluorescence background of Raman spectra for the two types of zircons were well
257 calibrated. After the calibration, the zircon Raman spectra vary from sharp peaks
258 (Sz3@04) of typical non-metamict zircons, to wide peaks (Sz2@01, Sz2@03) in
259 highly-metamict grains (Fig. 2c). To quantify the degree of zircon metamictization,
260 the FWHMs and Raman shifts of the $\nu_3(SiO_4)$ bands were measured.

261 Two types of Raman spectra, as exemplified by Sz2@01 (metamict) and Sz3@04
262 (crystalline), are shown in Figures 3a and 3b, respectively. The FWHM of metamict
263 zircon is significantly larger than that of non-metamict zircon. The Raman shift of the
264 $\nu_3(SiO_4)$ band in metamict zircons shifts to a lower wave number. To acquire the real
265 FWHM, the measured FWHM is corrected with the spectral resolution (Irmer, 1985),
266 which yielded 13.9 cm^{-1} (Sz2@01) and 6.4 cm^{-1} (Sz3@04). The real FWHMs are
267 negatively correlated with the Raman shifts (Fig. 3c; Table 1), consistent with what
268 was observed in previous work (Pidgeon et al., 2014). As the $\nu_3(SiO_4)$ Raman band
269 cannot be observed in some extremely-metamict zircons, and hence the above
270 Gaussian function fitting method is no longer applicable. In that case, the FWHMs
271 were set to the maximum value of 20 cm^{-1}. Raman shift and FWHM of each analysis
272 spot is listed in Supplementary Table 1.

Zircon water content and oxygen isotopes

When water content is very high, the electron multiplier protection will be triggered and $^{16}O^{1}H/^{16}O$ ratio will be zero. In this case, we set the water content to be 5000.0 ppm for further analyses (Supplementary Table 1). Water contents of the unscreened zircons from the four samples are highly dispersive (657–5118 ppm), particularly for the zircons from fine-grained granite Sz3 (Fig. 4a). Nevertheless, most data are clustered in the 680–1400 ppm range, and the median values of the four samples are similar (in the 1000–1500 ppm range; Fig. 4a). Likewise, the unscreened zircons show wide $\delta^{18}O$ range (4.0–6.1‰), most of which cluster around the mantle value (5.3 ± 0.6‰; Valley et al., 1998) (Fig. 4b). The majority of the sample Sz3 data have lower $\delta^{18}O$ values than that of the mantle. This discrepancy is possibly induced by a matrix effect due to zircon metamictization. The structure and mineralogy of metamict zircon will change the instrumental mass fractionation, which means further matrix correction is required while it is unavailable at present. There is a weak negative correlation between the zircon water content and non-matrix corrected $\delta^{18}O$ (Fig. 4c), but the correlation disappears when $\delta^{18}O$ >4.8‰, and the water content is below 1600 ppm (Fig. 4c).

Zircon trace element compositions

The Suzhou zircons show chondrite-normalized REE patterns typical of igneous zircons (Belousova et al., 2002), with enrichments in heavy REEs (HREE; Fig. 5; Supplementary Table 1). Light REE (LREE) contents in the zircons are variable. In Sz2 and Sz3, metamict zircons have higher LREE and HREE contents than their

non-metamict counterparts (Fig. 5b, c; Table 1), but such phenomenon is not found in the other two samples (Sz1, Sz4; Fig. 5a, d). The zircons have 30–9,071 ppm U and 22–6,237 ppm Th. In general, high U zircons have higher FWHMs (Fig. 5e-h; Table 1), total REE, and Hf (Fig. 5e, g; Table 1), but varying P contents (Fig. 5g). All the zircons show distinct negative Eu anomalies, which are negatively correlated with the U content (Fig. 5h; Table 1). Positive Ce anomalies are also observed, but they are weak in LREE-enriched zircons (Fig. 5a-b).

Discussion

Screening-criteria for least-metamict zircons

In the Suzhou A-type granites, the more-metamict zircons have lower $\delta^{18}O$ values but higher water content than non-metamict ones (Fig. 6a-b; Table 1; Gao et al., 2014). The lower-$\delta^{18}O$ values are likely caused by the absorption of atmospheric water in the metamict zircons (Gao et al. 2014), as supported by the negative $\delta^{18}O$ vs. H_2O-content correlation (Fig. 4c). In addition, the metamictization-induced matrix effect may have played an important role in the low-$\delta^{18}O$ measurements as well, which has been uncovered in zircon dating by previous studies (Allen and Campbell, 2012; Gao et al., 2014; White and Ireland, 2012).

Based on the Raman spectroscopy measured transition of crystal structure of zircon, Nasdala et al. (1995, 2001b) regarded the zircons with FWHMs <20 cm^{-1} as pristine crystals. Murakami et al. (1991) conducted X-ray diffraction (XRD) analysis on gem zircon from Sri Lankan, and found that when FWHMs <30 cm^{-1}, the crystal

damage is dominated by point defects, whereas radiation damage is scarce. These criteria are, however, unsuitable for zircon water content or oxygen isotope analyses because water contents in the Suzhou zircons (FWHM = 8–30 cm^{-1}) seem also to have been affected (Fig. 6a, c). Since higher FWHM and lower Raman shift correspond to higher zircon water contents and lower $\delta^{18}O$, respectively (Fig. 6), the analyses on metamict zircons may have overestimated the water contents but underestimated the $\delta^{18}O$ values.

Figure 6 shows the results of the widely-used decision tree regression, where a major change in zircon water content is observed when the FWHMs are above 8 cm^{-1} (Table 1), the Raman shifts above 1007 cm^{-1}, and the radiation dose (D_{dpa}) below 0.023 (calculated after Nasdala et al., 2001b). These values are likely the thresholds under/above which zircons tend to preserve their primary water. When the FWHMs <10 cm^{-1}, Raman shifts <1005.5 cm^{-1}, and D_{dpa} <0.03, most of the zircons are considered to preserve their primary oxygen isotope compositions (Fig. 6c, d). Likewise, these values can be taken as thresholds for reliable analyses of zircon primary oxygen isotopes. Therefore, we propose that for water measurement, the selection criteria for the least-metamict zircons are <8 cm^{-1} FWHMs, >1007 cm^{-1} Raman shifts, and <0.023 D_{dpa}. For oxygen isotope analysis, the selection criteria are <10 cm^{-1} FWHMs, >1005.5 cm^{-1} Raman shifts, and <0.03 D_{dpa}.

The feasibility of such a selection scheme is evaluated in Figure 4 and Table 1, which compares the measured water content and oxygen isotopes for the unscreened and screened Suzhou zircons. For a given sample, the screened zircons show a much

narrower and lower water content but higher $\delta^{18}O$ than the unscreened ones (Fig. 4a, b; Table 1). The most extreme example is sample Sz3, whose primary water content in the screened non-metamict zircons (681–1382 ppm) is significantly lower than that in the unscreened zircons (673–5118 ppm; Fig. 4a). Similarly, $\delta^{18}O$ values of the unscreened zircons (4.0–6.1‰) fall into a much wider range than the screened, non-metamict ones from the same sample (4.5–5.5‰) of (Fig. 4b). With this screening scheme, the primary water content (ca. 650–1400 ppm) and $\delta^{18}O$ (4.5–6.0‰) obtained are close to the mantle value (5.3 ± 0.6‰; Fig. 4a, b). A few analysis spots on the screened zircons show very high-water content and low-oxygen isotopes, probably reflecting decoupled analytical volumes for Raman and SIMS.

Previous studies show that metamict zircons have much higher REE, U and P concentrations, but lower LREE/HREE fractionation than non-metamict ones (Belousova et al., 2002; Horie et al., 2006). Metamict zircons also show weakly-negative or even positive Eu anomalies (Horie et al., 2006). Thus, trace element variations could potentially be used as proxies for the degree of metamictization. For instance, the total REE content increases with the metamictization intensity (Fig. 5e). However, P content does not show any correlation with U (Fig. 5f), and the extent of Eu anomalies correlates negatively with the U content (Fig. 5h), different from previous observations (Belousova et al., 2002; Horie et al., 2006). This implies that the zircon trace element variation cannot be influenced by metamictization alone. The positive correlation between zircon Hf, which is a proxy for magma evolution (Breiter et al., 2014), and U content (Fig. 5g; Table 1) indicates

that the trace element co-variation is more likely led by magma fractionation rather than metamictization. Consequently, trace elements are not good indicator for metamictization.

As discussed above, the FWHM threshold for water content is more restricted than that for oxygen isotope, indicating that primary water in zircon is more susceptible to radiation damage. The differences between these two criteria may be linked to the lower oxygen diffusion coefficient in zircon than that of hydrogen (Ingrin and Zhang, 2016; Watson and Cherniak, 1997; Zhang, 2015). It is noteworthy that the water contents in those metamict zircons with FWHMs in the range of 8–10 cm^{-1} are similar to those that in non-metamict zircons (Fig. 5a). As indicated by Woodhead et al. (1991), perhaps only part of the damaged zircons adsorbed appreciate amount of secondary water.

Significance of primary water content zircons in Suzhou A-type granites

The $\delta^{18}O$ values of our screened zircons are mantle-like, indicates a predominant mantle contribution to the Suzhou granites (Gao et al., 2014). However, their water content is much higher than that of the zircons from typical intraplate mantle-derived rocks (81–177 ppm) and continental-arc I-type granites (400–736 ppm) (Fig. 7; author's unpubl. data). A-type granites are commonly interpreted as products generated under anhydrous conditions (Clemens et al., 1986; Collins et al., 1982), and the high-water content of zircons from the Suzhou A-type granites may challenge this conventional view.

The measured primary water contents in zircon could be a result of diffused

original water. Nevertheless, diffusive loss of water implies zircon in A-type granite has higher original water content. In addition, finer granite generally cools faster, and could preserve the original water content in zircon. The different grain sizes of four samples in this study (coarse–porphyritic–fine), presumably cooled at different rates, display similar primary water content (Fig. 5a, b), suggesting negligible diffusion effect of post-zircon crystallization processes.

Pressure and temperature are additional factors that can influence the water content in zircon. Granites are formed largely in the crust and hence their formation pressure does not exceed ~1.5 GPa (Anderson, 1997; Johannes and Holtz, 2012). Under such conditions, the water content of NAMs correlates positively with pressure but negatively with temperature (Keppler, 2006; O'Leary et al., 2010), i.e., low-pressure and high-temperature granites should be “drier”. The Suzhou A-type granites were formed in an extensional environment, at shallower crustal depth (Charoy and Raimbault, 1994) but higher temperature than those of I-type granite (Clemens et al., 1986; Creaser et al., 1991). However, the median zircon water content of our samples (1018 ppm) is much higher than that of I-type granites (median 400–736 ppm; Fig. 7). This may argue against a major control of pressure and temperature on the zircon water content.

De Hoog et al. (2014) and Trail et al. (2010) suggested that the water partition coefficient between zircon and melt increases with REE content but decreases with increasing P content. If these generalizations hold in the first order, the zircon water content would correlate with trace element contents, which is not observed in our

406 samples (Fig. 8). Specifically, the molar REE+Y-P content in the Suzhou non-metamict
407 zircons varies, but the water content remains relatively stable (Fig. 8). In contrast,
408 zircons in the Penglai alkali basalt (Li et al., 2010) and Jurassic I-type granites in the
409 North China Craton (Wu et al., 2005; Yang et al., 2007) show limited variation in their
410 molar REE+Y-P, but extremely wide range in water content (Fig. 8; author's unpubl.
411 data). This suggests that the relations between water and trace element contents in
412 zircon is much more complex than previously thought.

413 It remains to assess whether the measured high-water contents in the Suzhou
414 zircons reflect the characteristics of primary granitic melts and of the source. In a
415 granitic system, zircon crystallizes over a large portion of magmatic history, but most
416 zircons crystallize at a short temperature interval immediately after reaching
417 saturation (Harrison et al., 2007; Samperton et al., 2017). Based on petrological
418 observation and experiments, Clemens et al. (1986) and Dall' Agnol et al. (1999)
419 argued that zircon in A-type granite crystallized during early stage of fractionation. In
420 the case of Suzhou A-type granites, zircons occur either interstitially (Charoy and
421 Raimbault, 1994; Wang et al., 1996) or as inclusions in other minerals (Wang et al.,
422 1993; Wang et al., 1996), pointing to a long zircon crystallization process. It is
423 therefore imperative to analyze early crystallized zircons in order to constrain the
424 water contents in primitive granitic magmas. Wang et al. (1993) showed that the
425 homogenization temperature of melt inclusions in larger zircons (>100 μm; ~930 ℃
426 to ~980 ℃) is much higher than that of smaller zircons (<100 μm, ~700 C°). The
427 early crystallized zircons also have generally lower Hf contents compared to late

crystallized ones, which often show higher Hf contents and low $\delta^{18}O$ due to hydrothermal alteration (Wei et al., 1999). The zircons selected for water measurement in this study are relatively large in size (mostly >100 μm) and show low Hf concentration and higher $\delta^{18}O$ (Table 1, Fig. 5g). They therefore most likely represent early crystallized zircons, which are not altered by late hydrothermal processes. Consequently, the measured high water contents in the Suzhou zircons reflect that of primary granitic melt. In fact, the Suzhou A-type granites are rich in fluids, as evidenced by the ubiquitous presence of fluids and mineral inclusions in zircon, as well as the common crystal cavities and pores (Charoy and Raimbault, 1994; Gao et al., 2014; Wang et al., 1993). It has long been believed that Suzhou granitic melts are mainly rich in volatiles such as F, but poor in water (Charoy and Raimbault, 1994; Wang et al., 1993). The data presented in this study, however, point to a hydrous character for the Suzhou granites, calling for a review of the A-type granite petrogenesis.

Implications

Metamictization exerts significant effects on water abundance in zircons and only unmetamictized zircons can preserve information about the primary water contents in the melts from which zircons crystallized. It is therefore imperative to select least-metamict zircons before proceeding to water analyses. In order to establish zircon screening criteria, investigation has been carried out on well-characterized Early Cretaceous Suzhou A-type granites using Raman spectrometer and SIMS. It is shown that the primary water content in zircon is least affected by metamictization

when the laser Raman spectra FWHMs are below 8 cm^{-1}, corresponding to Raman shift at 1007 cm^{-1}. For oxygen isotope analysis, the critical FWHMs range is 10 cm^{-1}, and the corresponding Raman shift is 1005.5 cm^{-1}. Some Suzhou zircons with anomalously high water contents are associated with low $\delta^{18}O$ values, probably resulting from absorbed meteoric water. The primary $\delta^{18}O$ in Suzhou zircons is of 4.5-6.0‰, indicating a predominant mantle contribution. The primary water content in the Suzhou zircons is of 650–1400 ppm, significantly higher than that of zircons in I-type granites and mantle-derived zircons. Sub-solidus diffusion, pressure, temperature and cation charge balance are not the controlling factors for the high primary water content in the Suzhou A-type granite, which is more likely related to the high-water content in melt, presenting a challenge to the traditional view on the "anhydrous" A-type granites and their genesis.

Acknowledgements

This study was supported by the National Natural Science Foundation of China (41688103, 41673010) and the Strategic Priority Research Program of the Chinese Academy of Sciences (XDB18000000). We thank Tan Dayong and Zhao Huifang for helping with the Raman spectroscopic analyses. We gratefully appreciate constructive reviews by Ryan Ickert and anonymous referee, and the editorial handling of the manuscript by Fangzhen Teng.

References cited

Aines, R.D., and Rossman, G.R. (1986) Relationships between Radiation-Damage

474 and Trace Water in Zircon, Quartz, and Topaz. American Mineralogist,
475 71(9-10), 1186-1193.
476 Allen, C.M., and Campbell, I.H. (2012) Identification and elimination of a
477 matrix-induced systematic error in LA–ICP–MS $^{206}Pb/^{238}U$ dating of zircon.
478 Chemical Geology, 332-333, 157-165.
479 Anderson, J.L. (1997) Status of thermobarometry in granitic batholiths. Earth and
480 Environmental Science Transactions of the Royal Society of Edinburgh,
481 87(1-2), 125-138.
482 Bell, E.A., Boehnke, P., and Mark Harrison, T. (2017) Applications of biotite
483 inclusion composition to zircon provenance determination. Earth and
484 Planetary Science Letters, 473, 237-246.
485 Belousova, E., Griffin, W., O'Reilly, S.Y., and Fisher, N. (2002) Igneous zircon: trace
486 element composition as an indicator of source rock type. Contributions to
487 Mineralogy and Petrology, 143(5), 602-622.
488 Breiter, K., Lamarão, C.N., Borges, R.M.K., and Dall'Agnol, R. (2014) Chemical
489 characteristics of zircon from A-type granites and comparison to zircon of
490 S-type granites. Lithos, 192-195, 208-225.
491 Burnham, A.D., and Berry, A.J. (2012) An experimental study of trace element
492 partitioning between zircon and melt as a function of oxygen fugacity.
493 Geochimica et Cosmochimica Acta, 95, 196-212.
494 Campbell, I.H., and Taylor, S.R. (1983) No Water, No Granites - No Oceans, No
495 Continents. Geophysical Research Letters, 10(11), 1061-1064.

Caruba, R., Baumer, A., Ganteaume, M., and Iacconi, P. (1985) An Experimental-Study of Hydroxyl-Groups and Water in Synthetic and Natural Zircons - a Model of the Metamict State. American Mineralogist, 70(11-12), 1224-1231.

Charoy, B., and Raimbault, L. (1994) Zr-, Th-, and Ree-Rich Biotite Differentiates in the A-type Granite Pluton of Suzhou (Eastern China): the Key Role of Fluorine. Journal of Petrology, 35(4), 919-962.

Chen, J.F., Foland, K.A., and Liu, Y.M. (1993) Precise ^{40}Ar-^{39}Ar dating of the suzhou composite granite. Acta Geologica Sinica, 9(1), 77-85.

Clemens, J.D., Holloway, J.R., and White, A.J.R. (1986) Origin of an A-type granite: Experimental constraints. American Mineralogist, 71(3-4), 317-324.

Clemens, J.D., Stevens, G., and Bryan, S.E. (2020) Conditions during the formation of granitic magmas by crustal melting – Hot or cold; drenched, damp or dry? Earth-Science Reviews, 200.

Collins, W.J., Beams, S.D., White, A.J.R., and Chappell, B.W. (1982) Nature and Origin of A-Type Granites with Particular Reference to Southeastern Australia. Contributions to Mineralogy and Petrology, 80(2), 189-200.

Collins, W.J., Murphy, J.B., Johnson, T.E., and Huang, H.Q. (2020) Critical role of water in the formation of continental crust. Nature Geoscience, 13(5), 331-338.

Creaser, R.A., Price, R.C., and Wormald, R.J. (1991) A-type granites revisited: Assessment of a residual-source model. Geology, 19(2), 163-166.

518 Davis, D.W., Krogh, T.E., and Williams, I.S. (2003) Historical Development of Zircon
519 Geochronology. Reviews in Mineralogy and Geochemistry, 53(1), 145-181.
520 De Hoog, J.C.M., Lissenberg, C.J., Brooker, R.A., Hinton, R., Trail, D., and
521 Hellebrand, E. (2014) Hydrogen incorporation and charge balance in natural
522 zircon. Geochimica et Cosmochimica Acta, 141, 472-486.
523 Ewing, R.C., Meldrum, A., Wang, L.M., Weber, W.J., and Corrales, L.R. (2003)
524 Radiation effects in zircon. Rev Mineral Geochem, 53, 387-425.
525 Fu, B., Page, F.Z., Cavosie, A.J., Fournelle, J., Kita, N.T., Lackey, J.S., Wilde, S.A.,
526 and Valley, J.W. (2008) Ti-in-zircon thermometry: applications and limitations.
527 Contributions to Mineralogy and Petrology, 156(2), 197-215.
528 Gaft, M., Panczer, G., Reisfeld, R., and Shinno, I. (2000) Laser-induced luminescence
529 of rare-earth elements in natural zircon. Journal of Alloys and Compounds,
530 300, 267-274.
531 Gao, Y.Y., Li, X.H., Griffin, W.L., O'Reilly, S.Y., and Wang, Y.F. (2014) Screening
532 criteria for reliable U–Pb geochronology and oxygen isotope analysis in
533 uranium-rich zircons: A case study from the Suzhou A-type granites, SE China.
534 Lithos, 192-195, 180-191.
535 Geisler, T., Ulonska, M., Schleicher, H., Pidgeon, R.T., and van Bronswijk, W. (2001)
536 Leaching and differential recrystallization of metamict zircon under
537 experimental hydrothermal conditions. Contributions to Mineralogy and
538 Petrology, 141(1), 53-65.
539 Griffin, W.L., Wang, X., Jackson, S.E., Pearson, N.J., O'Reilly, S.Y., Xu, X., and Zhou,

X. (2002) Zircon chemistry and magma mixing, SE China: In-situ analysis of Hf isotopes, Tonglu and Pingtan igneous complexes. Lithos, 61(3-4), 237-269.

Horie, K., Hidaka, H., and Gauthier-Lafaye, F. (2006) Elemental distribution in zircon: Alteration and radiation-damage effects. Physics and Chemistry of the Earth, Parts A/B/C, 31(10-14), 587-592.

Ingrin, J., and Zhang, P.P. (2016) Hydrogen diffusion in Zircon. EGU General Assembly Conference Abstracts, 18.

Irmer, G. (1985) On the influence of the apparatus function on the determination of scattering cross sections and lifetimes from optical phonon spectra. Experimentelle Technik der Physik, 33, 501-506.

Johannes, W., and Holtz, F. (1996) Petrogenesis and experimental petrology of granitic rocks. 335 p. Springer Science & Business Media, Berlin.

Kemp, A.I., Hawkesworth, C.J., Foster, G.L., Paterson, B.A., Woodhead, J.D., Hergt, J.M., Gray, C.M., and Whitehouse, M.J. (2007) Magmatic and crustal differentiation history of granitic rocks from Hf-O isotopes in zircon. Science, 315(5814), 980-3.

Keppler, H. (2006) Thermodynamics of Water Solubility and Partitioning. Reviews in Mineralogy and Geochemistry, 62(1), 193-230.

Li, X.H., Long, W.G., Li, Q.L., Liu, Y., Zheng, Y.F., Yang, Y.H., Chamberlain, K.R., Wan, D.F., Guo, C.H., Wang, X.C., and Tao, H. (2010) Penglai Zircon Megacrysts: A Potential New Working Reference Material for Microbeam Determination of Hf-O Isotopes and U-Pb Age. Geostandards and

562 Geoanalytical Research, 34(2), 117-134.

563 Li, X.H., Tang, G.Q., Gong, B., Yang, Y.H., Hou, K.J., Hu, Z.C., Li, Q.L., Liu, Y., and
564 Li, W.X. (2013) Qinghu zircon: A working reference for microbeam analysis
565 of U-Pb age and Hf and O isotopes. Chinese Science Bulletin, 58(36),
566 4647-4654.

567 Murakami, T., Chakoumakos, B.C., Ewing, R.C., Lumpkin, G.R., and Weber, W.J.
568 (1991) Alpha-Decay Event Damage in Zircon. American Mineralogist,
569 76(9-10), 1510-1532.

570 Nasdala, L., Beran, A., Libowitzky, E., and Wolf, D. (2001a) The incorporation of
571 hydroxyl groups and molecular water in natural zircon ($ZrSiO_4$). American
572 Journal of Science, 301(10), 831-857.

573 Nasdala, L., Irmer, G., and Wolf, D. (1995) The degree of metamictization in zircon: a
574 Raman-spectroscopic study. European Journal of Mineralogy, 7(3), 471-478.

575 Nasdala, L., Kronz, A., Wirth, R., Váczi, T., Pérez-Soba, C., Willner, A., and Kennedy,
576 A.K. (2009) The phenomenon of deficient electron microprobe totals in
577 radiation-damaged and altered zircon. Geochimica et Cosmochimica Acta,
578 73(6), 1637-1650.

579 Nasdala, L., Wenzel, M., Vavra, G., Irmer, G., Wenzel, T., and Kober, B. (2001b)
580 Metamictisation of natural zircon: accumulation versus thermal annealing of
581 radioactivity-induced damage. Contributions to Mineralogy and Petrology,
582 141(2), 125-144.

583 O'Leary, J.A., Gaetani, G.A., and Hauri, E.H. (2010) The effect of tetrahedral Al^{3+} on

584 the partitioning of water between clinopyroxene and silicate melt. Earth and
585 Planetary Science Letters, 297(1-2), 111-120.
586 Ouyang, X.W. (1985) The geochemical characteristics and petrogenesis of Suzhou
587 and Geyuan Granites. Institute of Geochemistry, MSc. Chinese Academy of
588 Sciences, Guiyang.
589 Pidgeon, R.T. (2014) Zircon radiation damage ages. Chemical Geology, 367, 13-22.
590 Pidgeon, R.T., Nemchin, A.A., and Cliff, J. (2013) Interaction of weathering solutions
591 with oxygen and U–Pb isotopic systems of radiation-damaged zircon from an
592 Archean granite, Darling Range Batholith, Western Australia. Contributions to
593 Mineralogy and Petrology, 166(2), 511-523.
594 Tang, M., Chu, X., Hao, J., and Shen, B. (2021) Orogenic quiescence in Earth's
595 middle age. Science, 371(6350), 728-731.
596 Tang, M., Lee, C.-T.A., Rudnick, R.L., and Condie, K.C. (2020) Rapid mantle
597 convection drove massive crustal thickening in the late Archean. Geochimica
598 et Cosmochimica Acta, 278, 6-15.
599 Trail, D., Bruce Watson, E., and Tailby, N.D. (2012) Ce and Eu anomalies in zircon as
600 proxies for the oxidation state of magmas. Geochimica et Cosmochimica Acta,
601 97, 70-87.
602 Trail, D., Thomas, J.B., and Watson, E.B. (2010) The incorporation of hydroxyl into
603 zircon. American Mineralogist, 96(1), 60-67.
604 Valley, J.W., Chiarenzelli, J.R., and McLelland, J.M. (1994) Oxygen isotope
605 geochemistry of zircon. Earth and Planetary Science Letters, 126(4), 187-206.

606 Valley, J.W., Kinny, P.D., Schulze, D.J., and Spicuzza, M.J. (1998) Zircon megacrysts
607 from kimberlite: oxygen isotope variability among mantle melts.
608 Contributions to Mineralogy and Petrology, 133(1-2), 1-11.
609 Wang, J.M., Yang, N.Q., Li, K.Q., and Ding, G.C. (1993) The metallogenesis and
610 magmatic differentiation of Suzhou A-type granite. Acta Petrologica Sinica,
611 9(01), 33-43.
612 Wang, R., Jeon, H., and Evans, N.J. (2018) Archaean hydrothermal fluid modified
613 zircons at Sunrise Dam and Kanowna Belle gold deposits, Western Australia:
614 Implications for post-magmatic fluid activity and ore genesis. American
615 Mineralogist, 103(12), 1891-1905.
616 Wang, R.C., Francois, F., Xu, S.J., Chen, X.M., and Pierre, M. (1996) Hafnian zircon
617 from the apical part of the Suzhou Granite, China. The Canadian Mineralogist,
618 34(5), 1001-1010.
619 Wang, X.L., Coble, M.A., Valley, J.W., Shu, X.J., Kitajima, K., Spicuzza, M.J., and
620 Sun, T. (2014) Influence of radiation damage on Late Jurassic zircon from
621 southern China: Evidence from in situ measurements of oxygen isotopes, laser
622 Raman, U–Pb ages, and trace elements. Chemical Geology, 389, 122-136.
623 Watson, E.B., and Cherniak, D.J. (1997) Oxygen diffusion in zircon. Earth and
624 Planetary Science Letters, 148, 527-544.
625 Watson, E.B., Wark, D.A., and Thomas, J.B. (2006) Crystallization thermometers for
626 zircon and rutile. Contributions to Mineralogy and Petrology, 151(4), 413-433.
627 Wei, C.S., Zhao, Z.F., and Spicuzza, M.J. (2008) Zircon oxygen isotopic constraint on

the sources of late Mesozoic A-type granites in eastern China. Chemical Geology, 250(1-4), 1-15.

White, L.T., and Ireland, T.R. (2012) High-uranium matrix effect in zircon and its implications for SHRIMP U–Pb age determinations. Chemical Geology, 306-307, 78-91.

Wilde, S.A., Valley, J.W., Peck, W.H., and Graham, C.M. (2001) Evidence from detrital zircons for the existence of continental crust and oceans on the Earth 4.4 Gyr ago. Nature, 409(6817), 175-8.

Woodhead, J.A., Rossman, G.R., and Silver, L.T. (1991a) The metamictization of zircon: radiation dose-dependent structural characteristics. American Mineralogist, 76(1-2), 74-82.

Woodhead, J.A., Rossman, G.R., and Thomas, A.P. (1991b) Hydrous species in zircon. American Mineralogist, 76(9-10), 1533-1546.

Wu, F.Y., Yang, J.H., Wilde, S.A., and Zhang, X.O. (2005) Geochronology, petrogenesis and tectonic implications of Jurassic granites in the Liaodong Peninsula, NE China. Chemical Geology, 221(1-2), 127-156.

Xia, X.P., Cui, Z.X., Li, W.C., Zhang, W.F., Yang, Q., Hui, H.J., and Lai, C.K. (2019) Zircon water content: reference material development and simultaneous measurement of oxygen isotopes by SIMS. Journal of Analytical Atomic Spectrometry.

Yang, J.H., Wu, F.Y., Liu, X.M., Xie, L.W., and Yang, Y.H. (2007) Petrogenesis and geological significance of the Jurassic Xiaoheishan pluton in the Liaodong

peninsula, east China: In-situ zircon U-Pb dating and Hf isotopic analysis. Bulletin of Mineralogy, Petrology and Geochemistry, 26(1), 29-43.

Zhang, L., Ren, Z.Y., Xia, X.P., Yang, Q., Hong, L.B., and Wu, D. (2019) In situ determination of trace elements in melt inclusions using laser ablation inductively coupled plasma sector field mass spectrometry. Rapid Commun Mass Spectrom, 33(4), 361-370.

Zhang, M., Salje, E.K.H., Capitani, G.C., Leroux, H., Clark, A.M., Schlüter, J., and Ewing, R.C. (2000) Annealing of alpha-decay damage in zircon: a Raman spectroscopic study. Journal of Physics: Condensed Matter, 12(13), 3131-3148.

Zhang, M., Salje, E.K.H., and Ewing, R.C. (2010) OH species, U ions, and CO/CO_2 in thermally annealed metamict zircon ($ZrSiO_4$). American Mineralogist, 95(11-12), 1717-1724.

Zhang, P.P. (2015) Hydrogen diffusion in NAMs: andradite garnet and zircon. Unité Matériaux et Transformations, Dortor of Philosophy, p. 218. Université de Lille.

Zhang, W.F., Xia, X.P., Eiichi, T., Li, L., Yang, Q., Zhang, Y.Q., Yang, Y.N., Liu, M.L., and Lai, C. (2020) Optimization of SIMS analytical parameters for water content measurement of olivine. Surface and Interface Analysis, 52(5), 224-233.

Zhang, W.F., Xia, X.P., Zhang, Y.Q., Peng, T.P., and Yang, Q. (2018) A novel sample preparation method for ultra-high vacuum (UHV) secondary ion mass

672 spectrometry (SIMS) analysis. Journal of Analytical Atomic Spectrometry,
673 33(9), 1559-1563.
674 Zou, X.Y., Qin, K.Z., Han, X.L., Li, G.M., Evans, N.J., Li, Z.Z., and Yang, W. (2019)
675 Insight into zircon REE oxy-barometers: A lattice strain model perspective.
676 Earth and Planetary Science Letters, 506, 87-96.
677

678 **Table 1.** Summary of Laser Raman spectra, SIMS water contents and oxygen isotope
679 compositions, and LA-ICP-MS trace element concentrations of zircons

680

681 **Figure captions**

682 **Figure 1.** Cathodoluminescence (CL) images of zircons from the Suzhou A-type
683 granites. Red and green circles mark the spots of SIMS and LA-ICP-MS analyses,
684 respectively.

685

686 **Figure 2. (a)** and **(b)** Raman spectra of typical highly-metamict (Sz2@01) and
687 non-metamict (Sz3@04) zircons. Black, green, and red solid lines denote the
688 measured spectra, baseline, and baseline-corrected spectra, respectively; **(c)**
689 Baseline-corrected Raman spectra of zircons with different degrees of
690 metamictization. $\nu_1(SiO_4)$ and $\nu_3(SiO_4)$ denote the Si-O tetrahedral symmetric and
691 antisymmetric stretching vibration mode, respectively.

692

693 **Figure 3. (a)** and **(b)** Enlarged Raman spectra of Sz2@01 and Sz3@04. Black and red
694 solid lines denote the Raman spectra after baseline correction and the Gaussian
695 function fitted to the $\nu_3(SiO_4)$ vibration band, respectively; **(c)** Correlation plot
696 between Raman shift and FWHM. Red circle marks the outlier.

697

698 **Figure 4. (a)** and **(b)** Box plots of zircon water contents and $\delta^{18}O$ distribution of the
699 four samples. Red solid lines in the box mark the median value positions. The

unscreened and screened data are shown in orange and blue, respectively; **(c)** Zircon H_2O vs. $\delta^{18}O$ plot. Negative correlation trend is present when $\delta^{18}O$ <~4.8‰, and disappears when $\delta^{18}O$ >~4.8‰.

Figure 5. (a-d) Chondrite-normalized REE patterns of zircons from the Suzhou granites. Colored and gray lines denote the non-metamict (FWHMs <8 cm^{-1}) and metamict (FWHMs >8 cm^{-1}) zircons, respectively; **(e-h)** Plots of total REE, P, Hf contents and Eu anomalies versus U content. Different colors show different FWHM magnitudes.

Figure 6. Zircon water content **(a, b)**, $\delta^{18}O$ **(c, d)** versus FWHM and Raman shift: **(a)** analysis spots with FWHM <8 cm^{-1}, 8–10 cm^{-1}, and >10 cm^{-1} are labeled in orange, blue and red, respectively. Blue solid line shows the result of tree regression on the medians, and the dark gray area shows the regression of 90% prediction interval. Inverted red triangles denote the thresholds of FWHMs and Raman shifts for the water content and $\delta^{18}O$ affected by metamictization.

Figure 7. Comparison of water content estimates for zircons from different tectonic settings. The Penglai zircons are from the Hainan Island alkaline basalts (Li et al., 2010) and Qinghu zircons are from mantle-derived monzonite in Nanling Range (Li et al., 2013), both formed in intraplate setting. Gangdese zircons are from the Late Cretaceous Gangdese I-type granites. NCC J1, NCC J3 and NCC K1 denote the Early

722 Jurassic, Late Jurassic and Early Cretaceous Liaodong continental arc I-type granites,
723 respectively. The data (except for Suzhou granites) are from authors' unpublished data.
724 Red solid line and the number on it denote the median location and value, respectively.
725 S and N denote the number of samples and analyzed spots, respectively.

726

727 **Figure 8.** Plot of zircon H_2O vs. (REE+Y-P) molar content. Blue circle denotes
728 zircons from Jurassic I-type granites in the North China Craton (unpubl. data). The
729 Penglai zircons from alkali basalt are shown in green (unpubl. data). Orange and gray
730 circles denote the non-metamict and metamict zircons of Suzhou A-type granites,
731 respectively.

732

This is the peer-reviewed, final accepted version for American Mineralogist, published by the Mineralogical Society of America.
The published version is subject to change. Cite as Authors (Year) Title. American Mineralogist, in press.
DOI: https://doi.org/10.2138/am-2022-8075. http://www.minsocam.org/

Table 1 Summary of Laser Raman spectra, SIMS water contents and oxygen isotope compositions, and LA-ICP-MS trace element concentrations of zircons

Sample	Type	FWHM (cm^{-1})	Raman shift (cm^{-1})	H_2O (ppm)	$\delta^{18}O$ (‰)	P (ppm)	Yb (ppm)	Hf (ppm)	U (ppm)	Total REE (ppm)	Eu/Eu*
Sz1	Crystalline	7.6	1007.4	732.0	5.56	201	424	6590	115	2300	0.048
Porphyritic granite	Crystalline	7.2	1007.4	777.8	5.15	126	243	9555	190	1274	0.032
	Metamict	17.1	999.8	4066.8	4.39	347	1401	10741	1876	7114	0.011
	Metamict	15.6	999.3	2882.2	4.46	204	649	6619	138	3921	0.084
Sz2	Crystalline	7.6	1006.8	1153.2	5.73	29870	11240	8884	656	128428	0.041
Coarse-grained granite	Crystalline	7.4	1007.4	657.6	5.81	208	648	6215	111	3715	0.112
	Metamict	13.9	1001.6	1045.4	4.89	271	1607	13279	2071	7485	0.009
	Metamict	17.5	1000.8	3520.7	4.72	359	1277	13510	2274	57825	0.014
Sz3	Crystalline	6.4	1008.2	686.1	5.56	134	296	5437	29.7	1796	0.264
Fine-grained granite	Crystalline	7.1	1007.8	888.8	5.23	416	346	6746	73.2	1750	0.122
	Metamict	19.4	999.1	3117.9	4.18	447	3315	13108	4445	15557	0.005
	Metamict	19.4	1000.2	2312.5	4.42	412	2562	13586	3467	11658	0.006
Sz4	Crystalline	7.8	1007.4	1011.6	4.99	228	787	6483	202	4754	0.042
Coarse-grained granite	Crystalline	7.4	1006.7	1179.0	5.32	2090	366	7623	146	3274	0.030
	Metamict	11.0	1005.0	1786.1	4.64	1337	638	9006	350	3690	0.047
	Metamict	12.0	1007.0	1428.6	4.52	11716	1203	7304	579	7911	0.115

This is the peer-reviewed, final accepted version for American Mineralogist, published by the Mineralogical Society of America.
The published version is subject to change. Cite as Authors (Year) Title. American Mineralogist, in press.
DOI: https://doi.org/10.2138/am-2022-8075. http://www.minsocam.org/

Figure 1

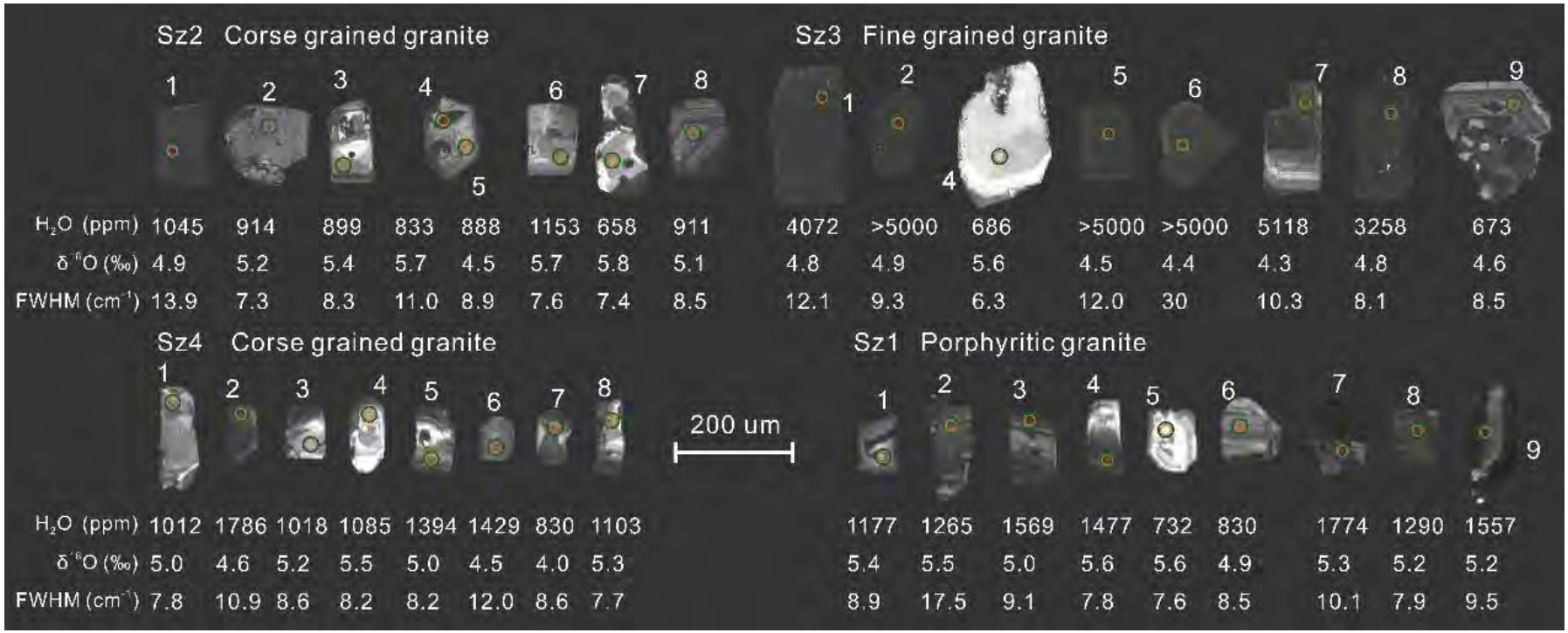

This is the peer-reviewed, final accepted version for American Mineralogist, published by the Mineralogical Society of America.
The published version is subject to change. Cite as Authors (Year) Title. American Mineralogist, in press.
DOI: https://doi.org/10.2138/am-2022-8075. http://www.minsocam.org/

Figure 2

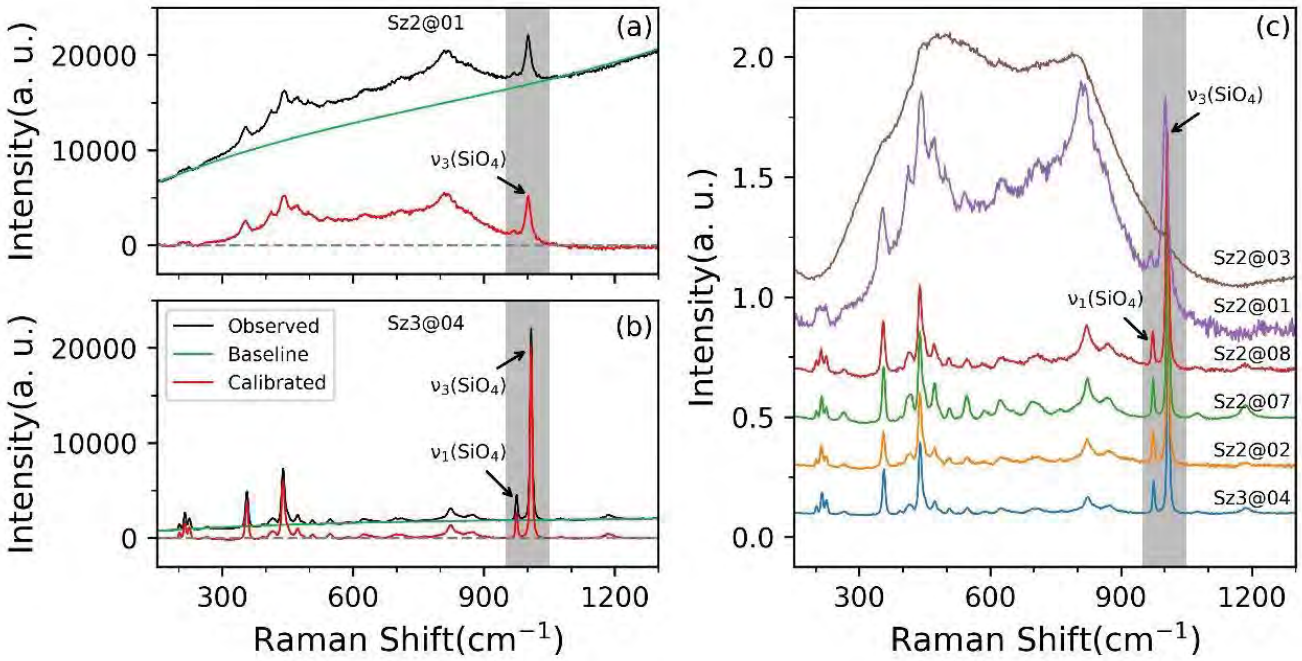

This is the peer-reviewed, final accepted version for American Mineralogist, published by the Mineralogical Society of America.
The published version is subject to change. Cite as Authors (Year) Title. American Mineralogist, in press.
DOI: https://doi.org/10.2138/am-2022-8075. http://www.minsocam.org/

Figure 3

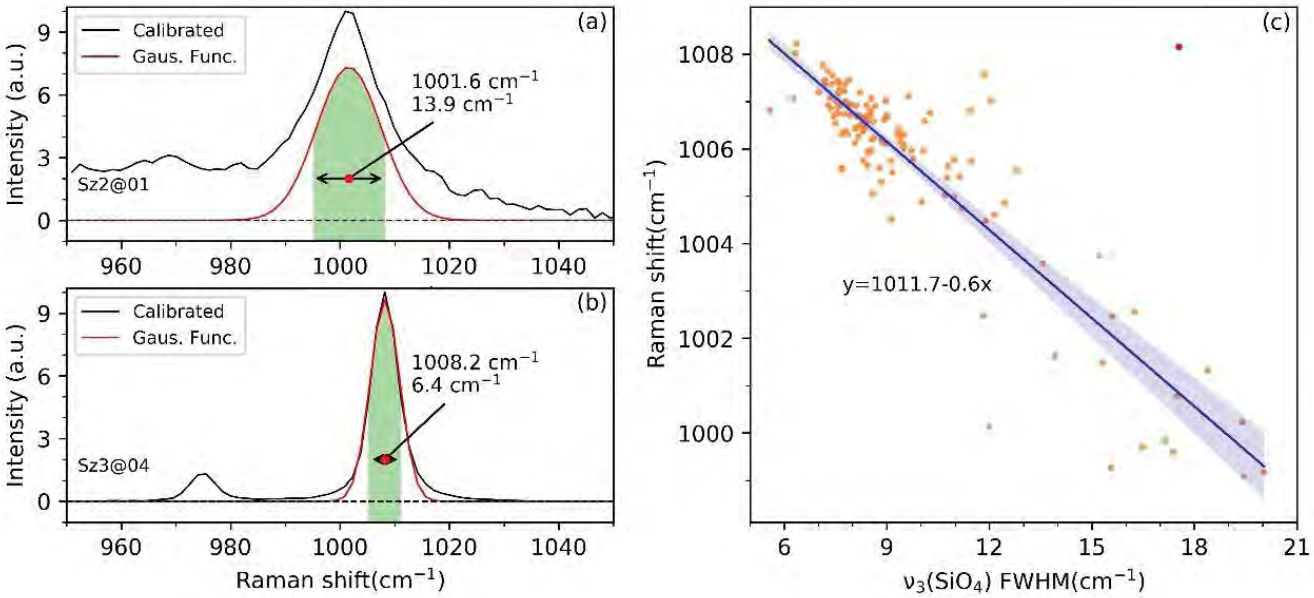

This is the peer-reviewed, final accepted version for American Mineralogist, published by the Mineralogical Society of America.
The published version is subject to change. Cite as Authors (Year) Title. American Mineralogist, in press.
DOI: https://doi.org/10.2138/am-2022-8075. http://www.minsocam.org/

Figure 4

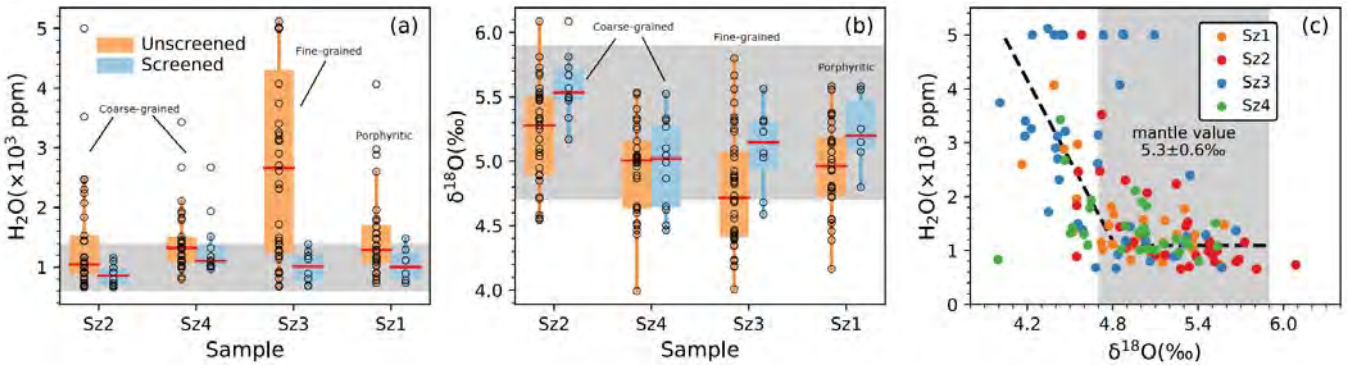

This is the peer-reviewed, final accepted version for American Mineralogist, published by the Mineralogical Society of America.
The published version is subject to change. Cite as Authors (Year) Title. American Mineralogist, in press.
DOI: https://doi.org/10.2138/am-2022-8075. http://www.minsocam.org/

Figure 5

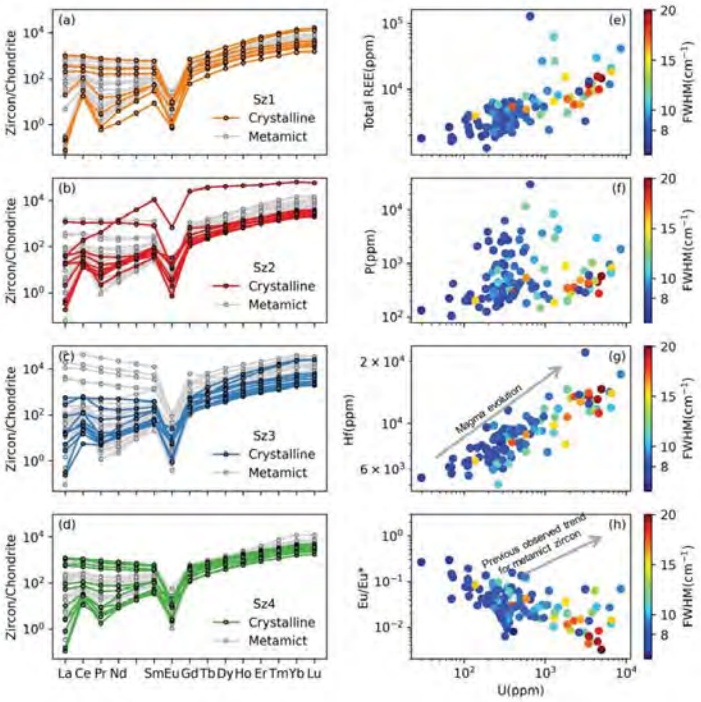

This is the peer-reviewed, final accepted version for American Mineralogist, published by the Mineralogical Society of America.
The published version is subject to change. Cite as Authors (Year) Title. American Mineralogist, in press.
DOI: https://doi.org/10.2138/am-2022-8075. http://www.minsocam.org/

Figure 6

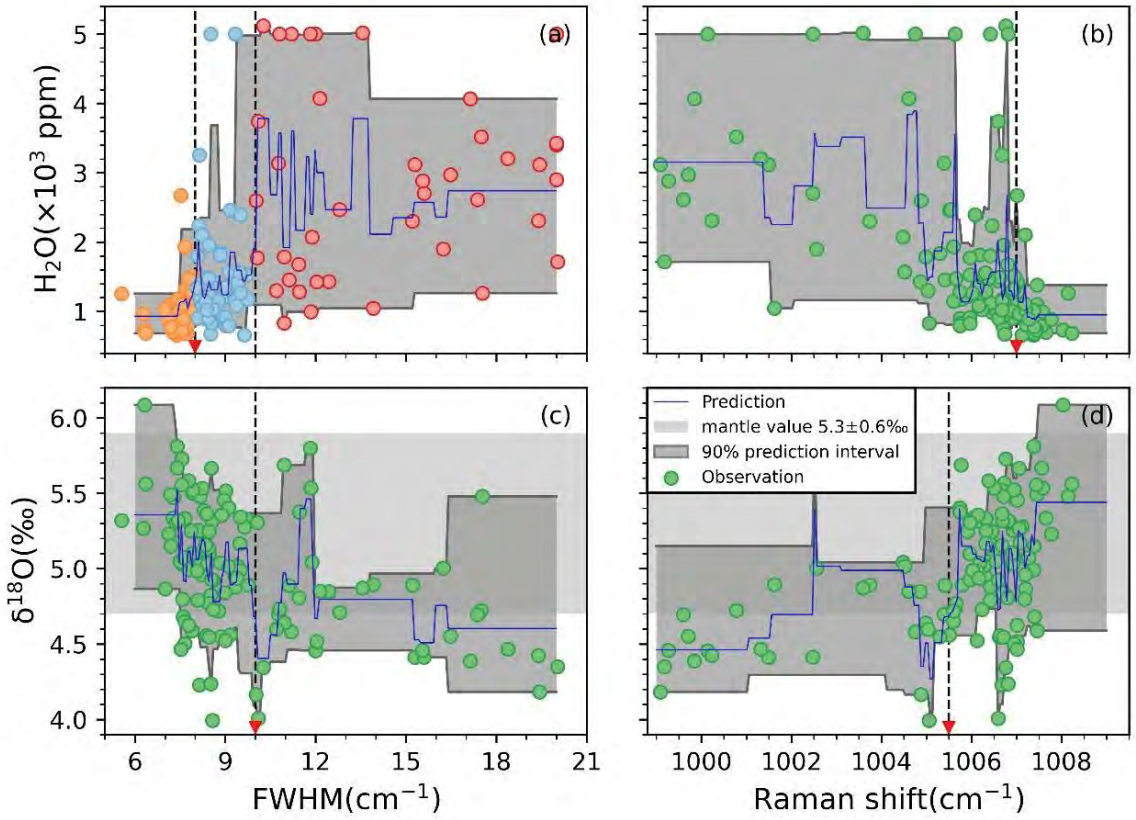

This is the peer-reviewed, final accepted version for American Mineralogist, published by the Mineralogical Society of America.
The published version is subject to change. Cite as Authors (Year) Title. American Mineralogist, in press.
DOI: https://doi.org/10.2138/am-2022-8075. http://www.minsocam.org/

Figure 7

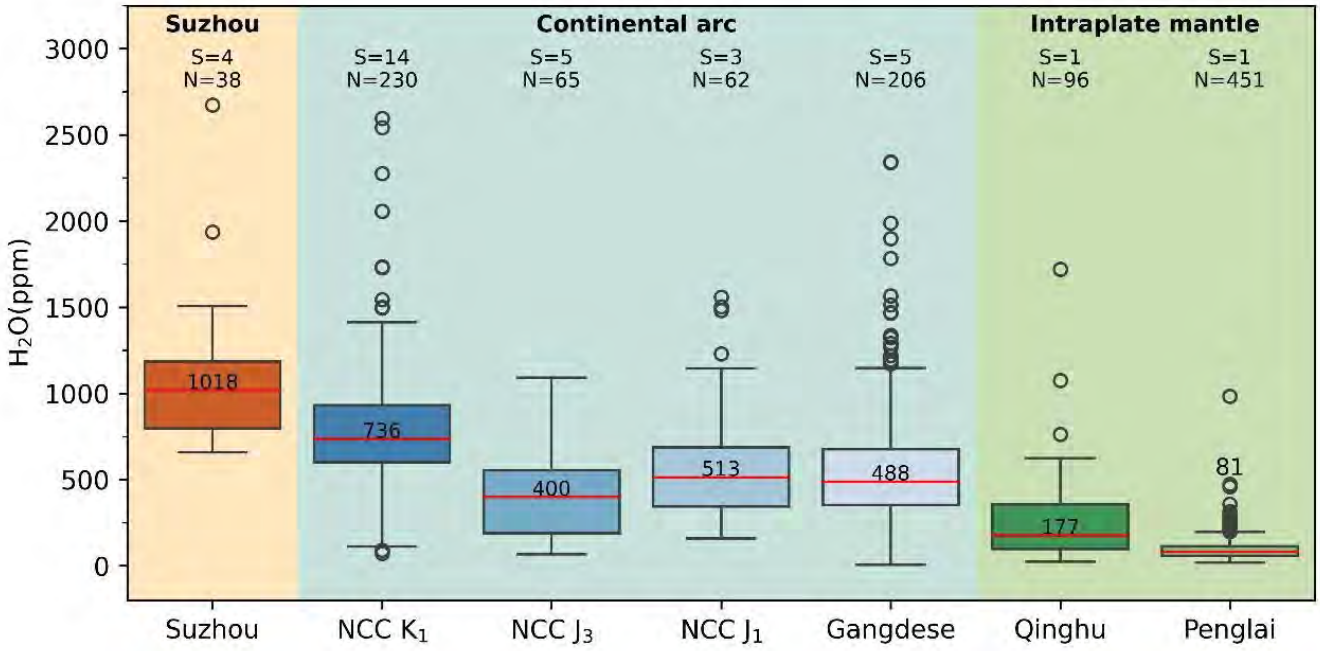

This is the peer-reviewed, final accepted version for American Mineralogist, published by the Mineralogical Society of America.
The published version is subject to change. Cite as Authors (Year) Title. American Mineralogist, in press.
DOI: https://doi.org/10.2138/am-2022-8075. http://www.minsocam.org/

Figure 8

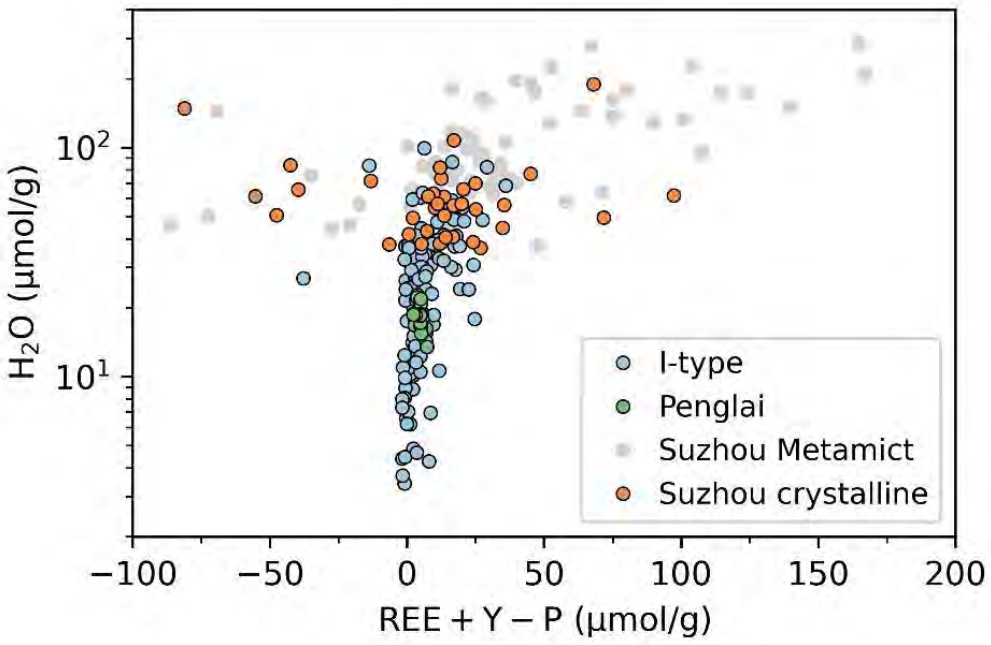

This is the peer-reviewed, final accepted version for American Mineralogist, published by the Mineralogical Society of America.
The published version is subject to change. Cite as Authors (Year) Title. American Mineralogist, in press.
DOI: https://doi.org/10.2138/am-2022-8075. http://www.minsocam.org/

Figure 3

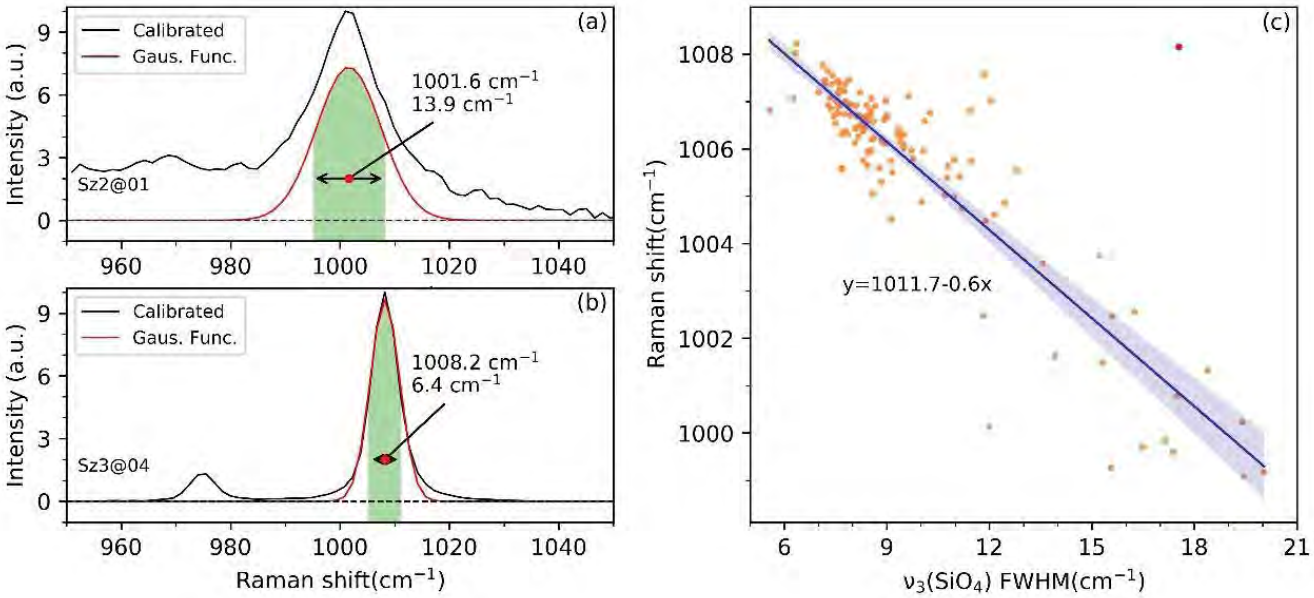

This is the peer-reviewed, final accepted version for American Mineralogist, published by the Mineralogical Society of America.
The published version is subject to change. Cite as Authors (Year) Title. American Mineralogist, in press.
DOI: https://doi.org/10.2138/am-2022-8075. http://www.minsocam.org/

Figure 4

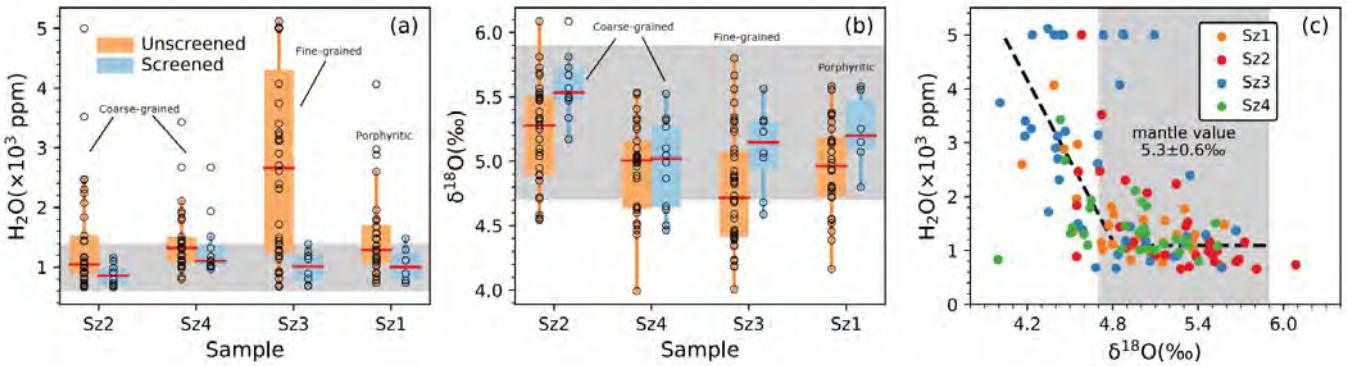

This is the peer-reviewed, final accepted version for American Mineralogist, published by the Mineralogical Society of America.
The published version is subject to change. Cite as Authors (Year) Title. American Mineralogist, in press.
DOI: https://doi.org/10.2138/am-2022-8075. http://www.minsocam.org/

Figure 5

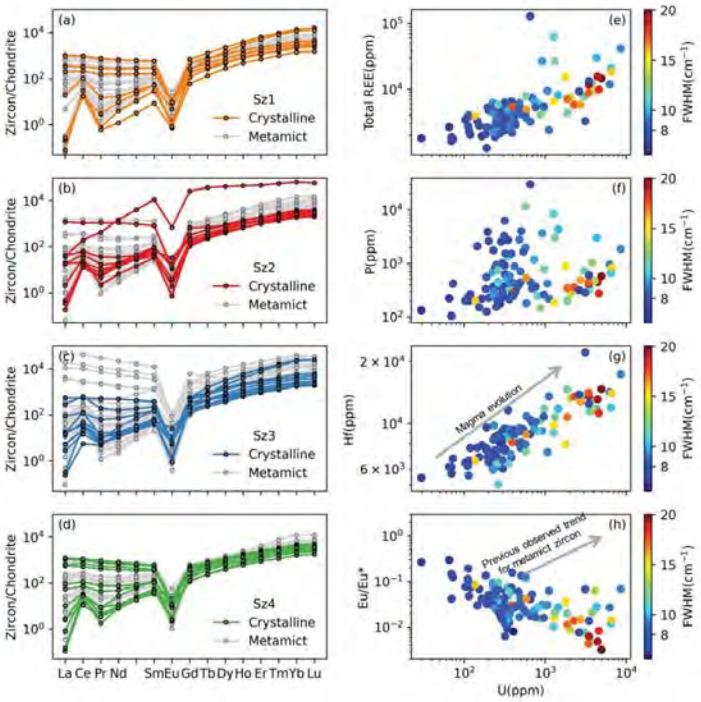

This is the peer-reviewed, final accepted version for American Mineralogist, published by the Mineralogical Society of America.
The published version is subject to change. Cite as Authors (Year) Title. American Mineralogist, in press.
DOI: https://doi.org/10.2138/am-2022-8075. http://www.minsocam.org/

Figure 6

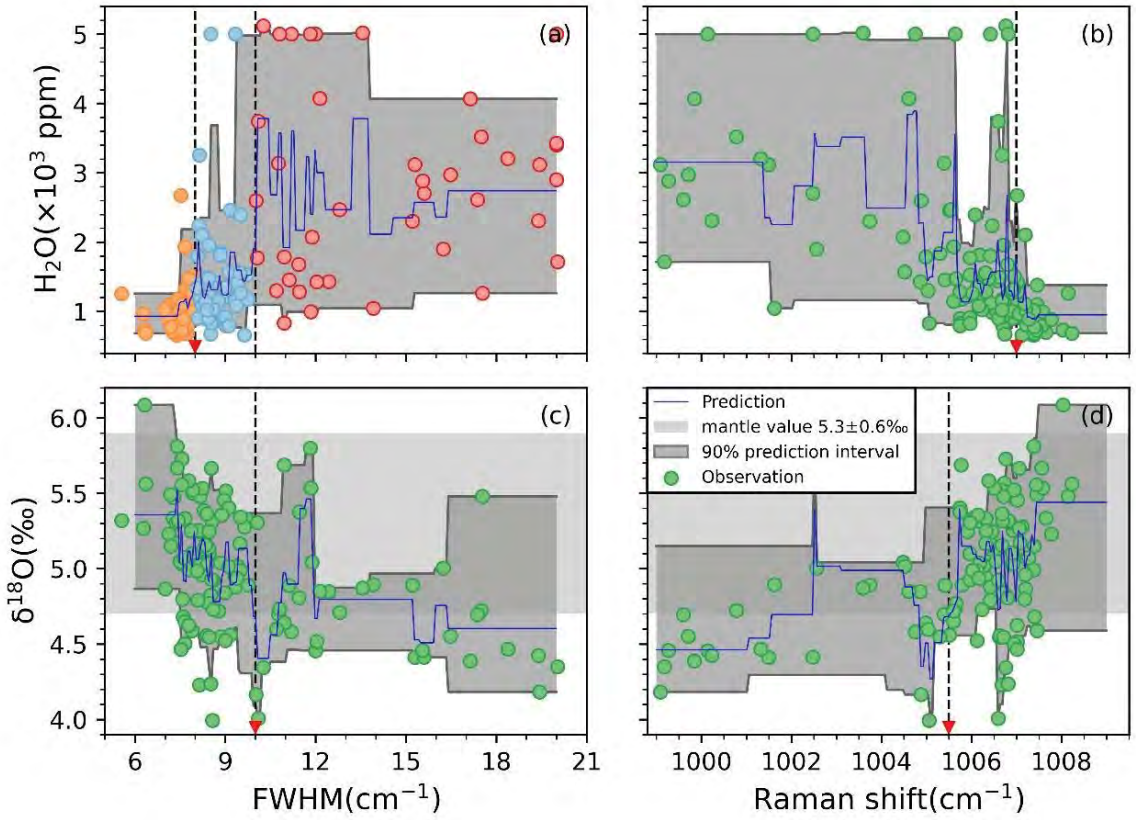

This is the peer-reviewed, final accepted version for American Mineralogist, published by the Mineralogical Society of America.
The published version is subject to change. Cite as Authors (Year) Title. American Mineralogist, in press.
DOI: https://doi.org/10.2138/am-2022-8075. http://www.minsocam.org/

Figure 7

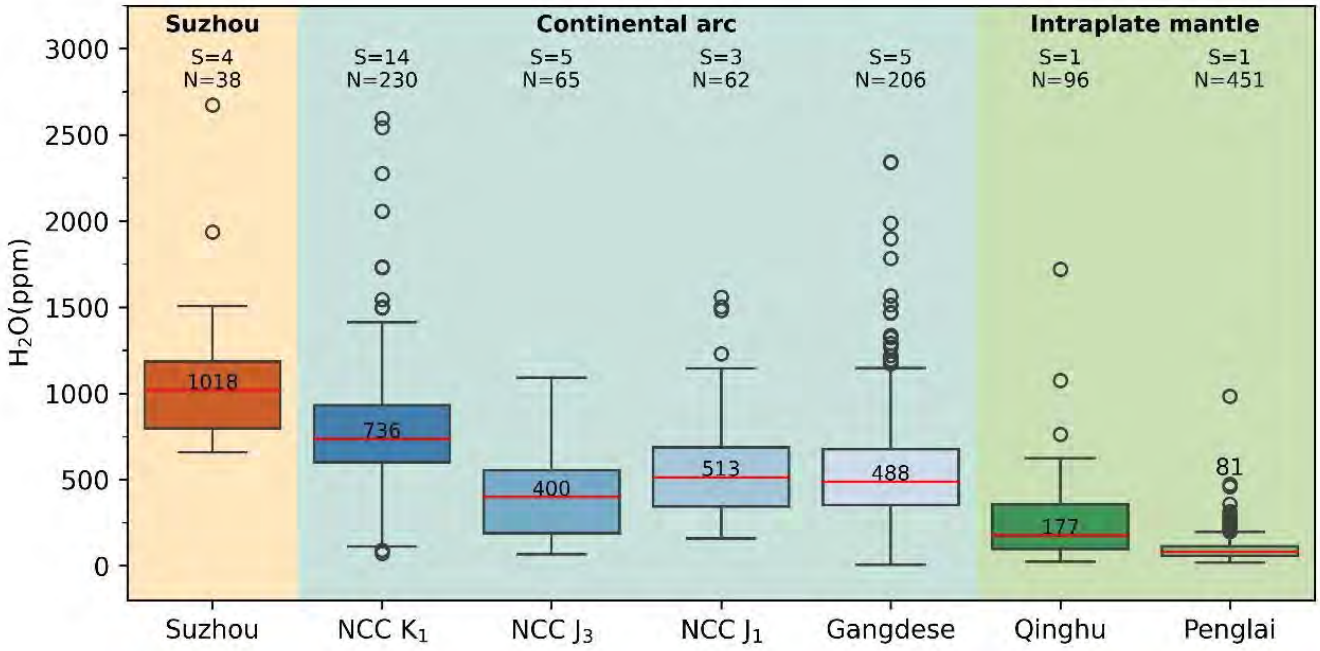

This is the peer-reviewed, final accepted version for American Mineralogist, published by the Mineralogical Society of America.
The published version is subject to change. Cite as Authors (Year) Title. American Mineralogist, in press.
DOI: https://doi.org/10.2138/am-2022-8075. http://www.minsocam.org/

Figure 8

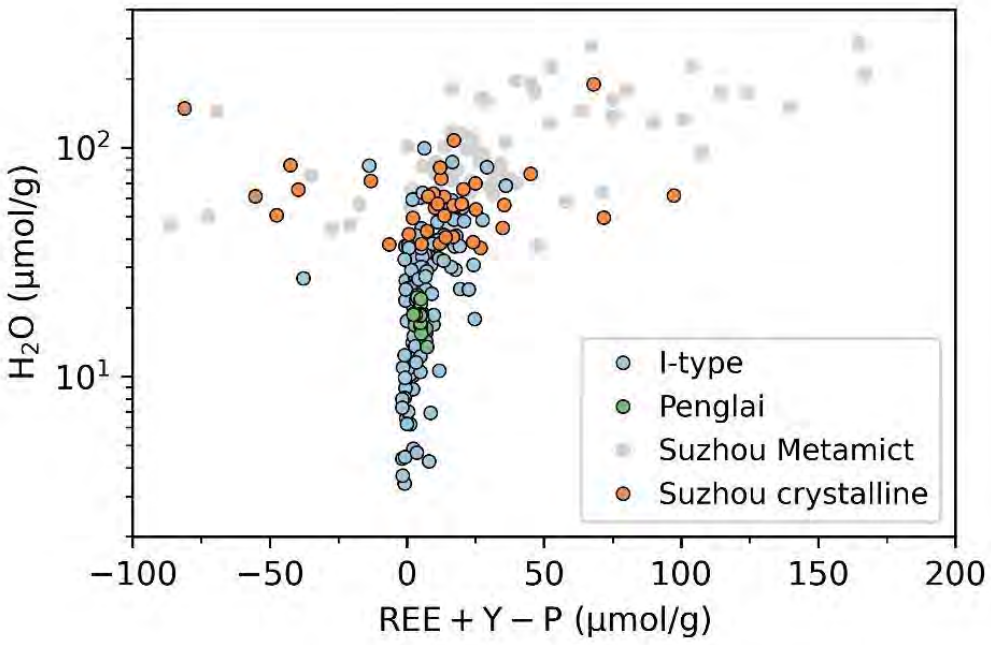

This is the peer-reviewed, final accepted version for American Mineralogist, published by the Mineralogical Society of America.
The published version is subject to change. Cite as Authors (Year) Title. American Mineralogist, in press.
DOI: https://doi.org/10.2138/am-2022-8075. http://www.minsocam.org/

Figure 4

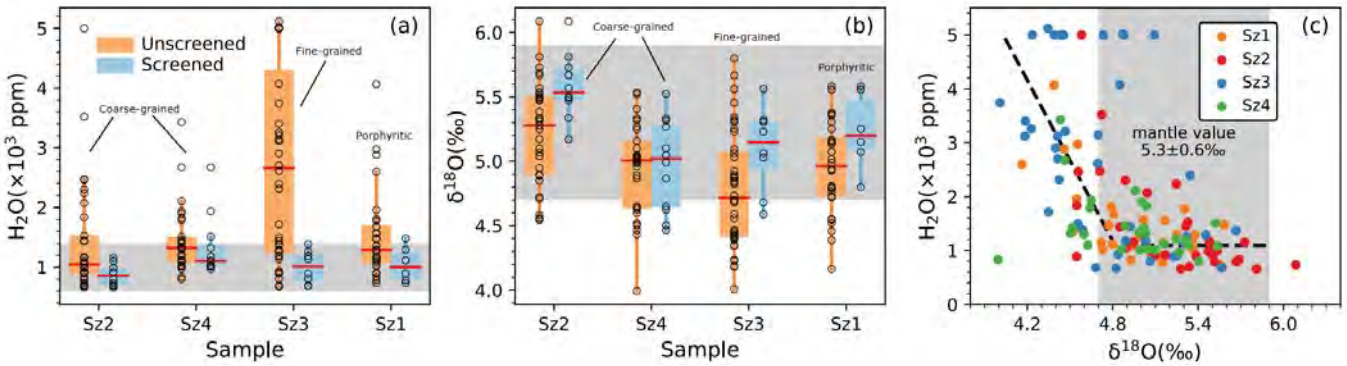

This is the peer-reviewed, final accepted version for American Mineralogist, published by the Mineralogical Society of America.
The published version is subject to change. Cite as Authors (Year) Title. American Mineralogist, in press.
DOI: https://doi.org/10.2138/am-2022-8075. http://www.minsocam.org/

Figure 5

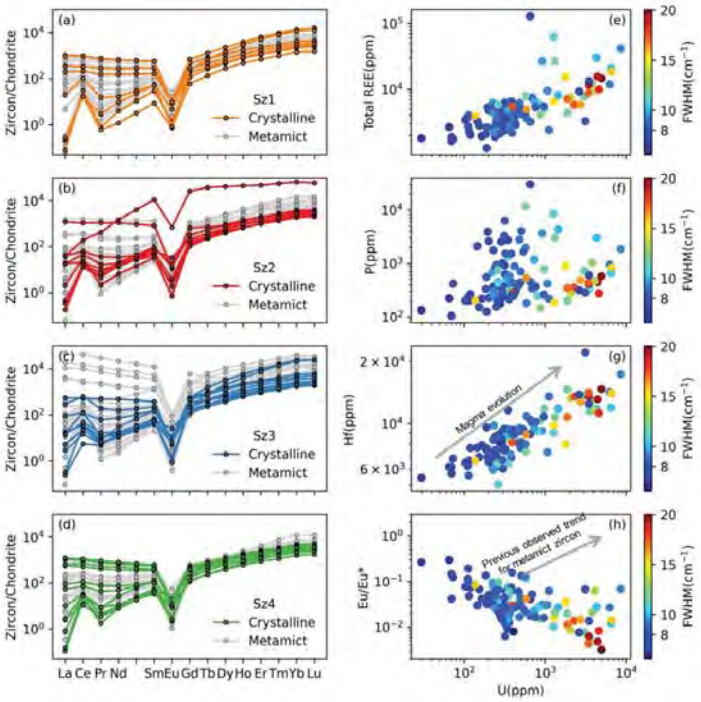

This is the peer-reviewed, final accepted version for American Mineralogist, published by the Mineralogical Society of America.
The published version is subject to change. Cite as Authors (Year) Title. American Mineralogist, in press.
DOI: https://doi.org/10.2138/am-2022-8075. http://www.minsocam.org/

Figure 6

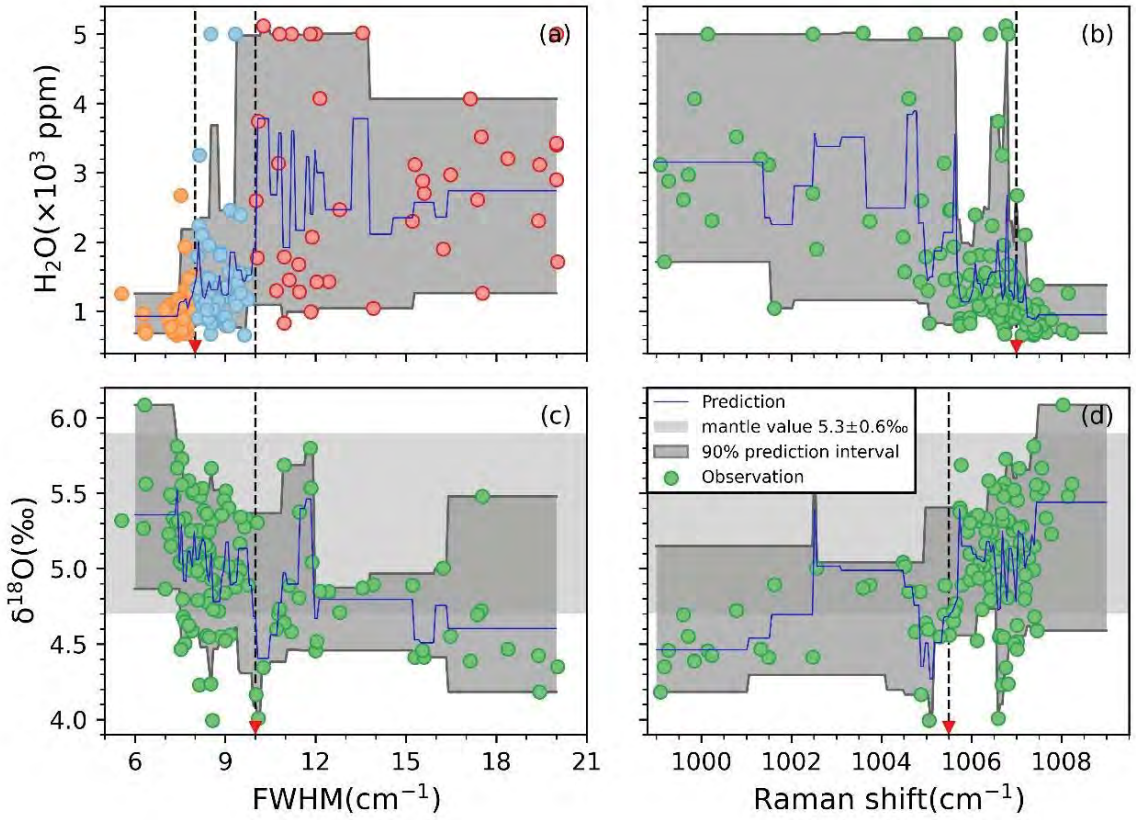

This is the peer-reviewed, final accepted version for American Mineralogist, published by the Mineralogical Society of America.
The published version is subject to change. Cite as Authors (Year) Title. American Mineralogist, in press.
DOI: https://doi.org/10.2138/am-2022-8075. http://www.minsocam.org/

Figure 7

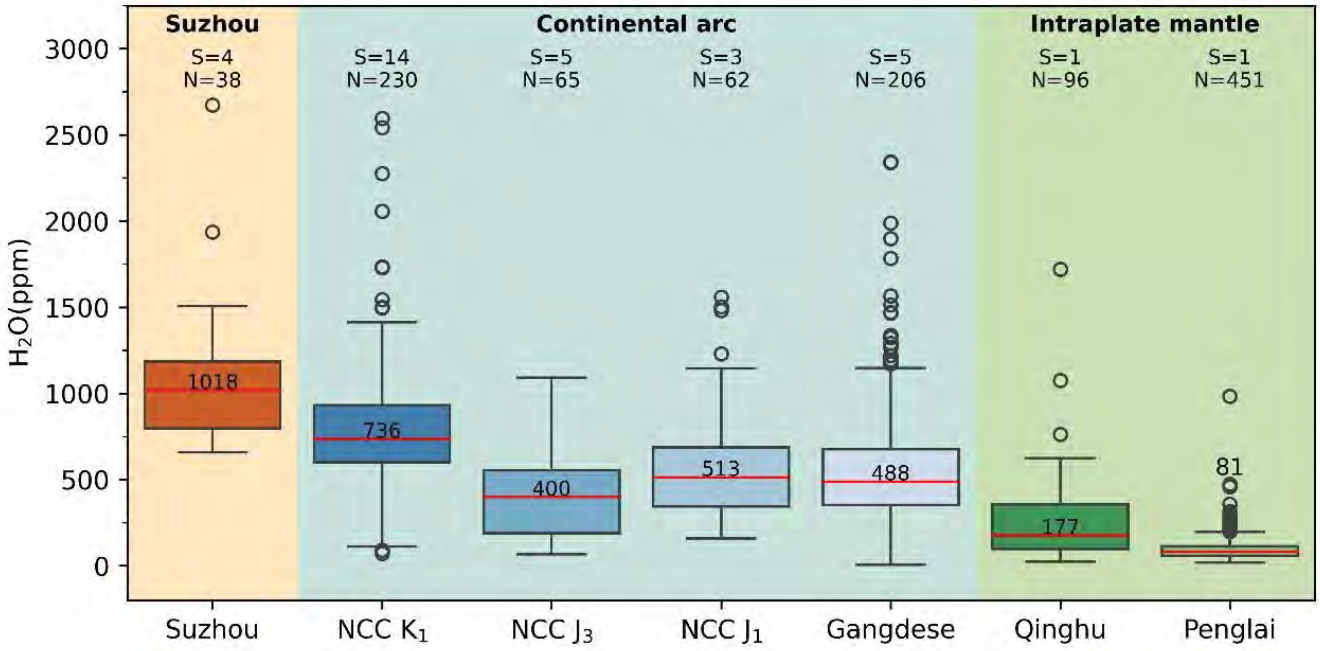

This is the peer-reviewed, final accepted version for American Mineralogist, published by the Mineralogical Society of America.
The published version is subject to change. Cite as Authors (Year) Title. American Mineralogist, in press.
DOI: https://doi.org/10.2138/am-2022-8075. http://www.minsocam.org/

Figure 8

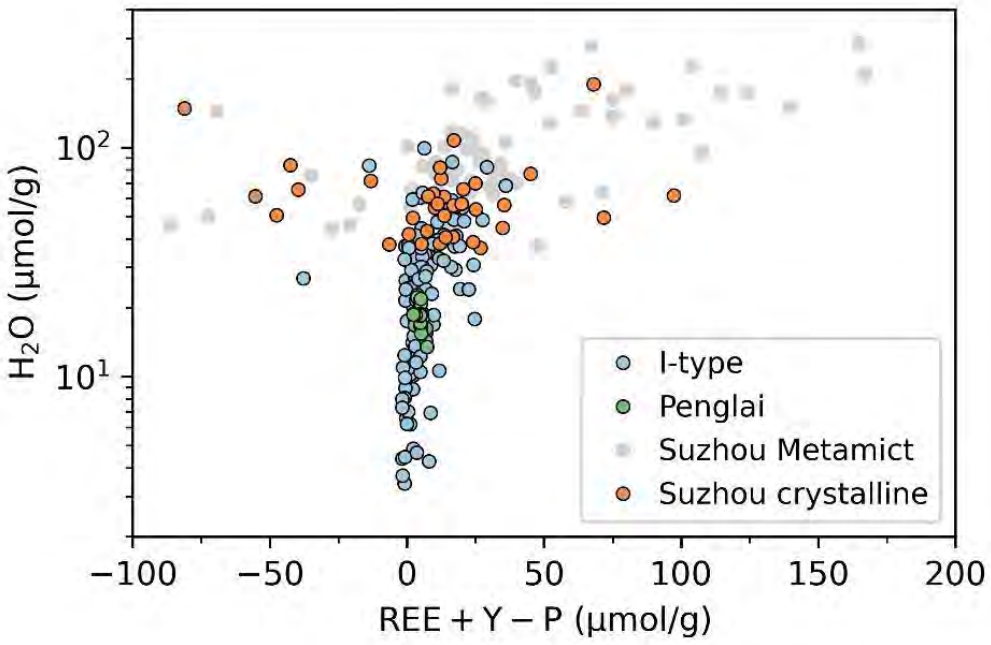

This is the peer-reviewed, final accepted version for American Mineralogist, published by the Mineralogical Society of America.
The published version is subject to change. Cite as Authors (Year) Title. American Mineralogist, in press.
DOI: https://doi.org/10.2138/am-2022-8075. http://www.minsocam.org/

Figure 4

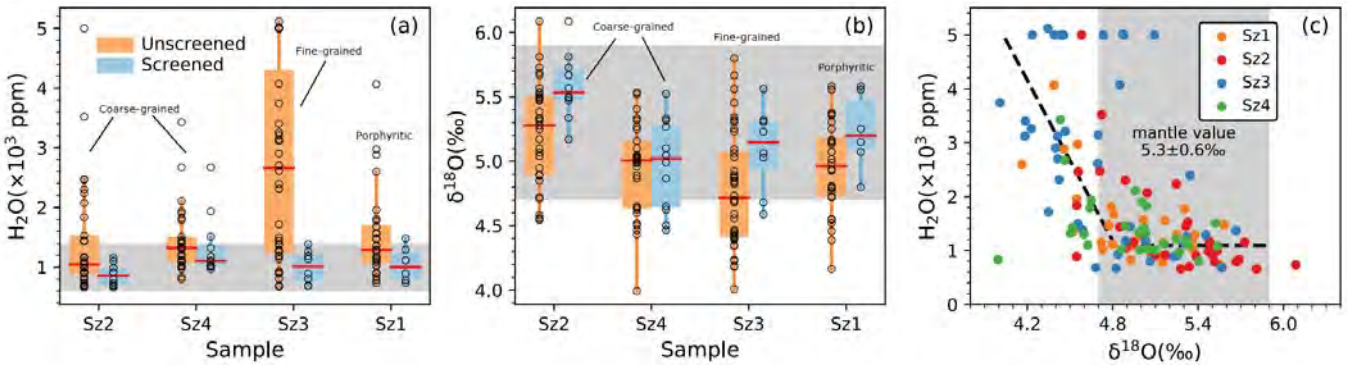

This is the peer-reviewed, final accepted version for American Mineralogist, published by the Mineralogical Society of America.
The published version is subject to change. Cite as Authors (Year) Title. American Mineralogist, in press.
DOI: https://doi.org/10.2138/am-2022-8075. http://www.minsocam.org/

Figure 5

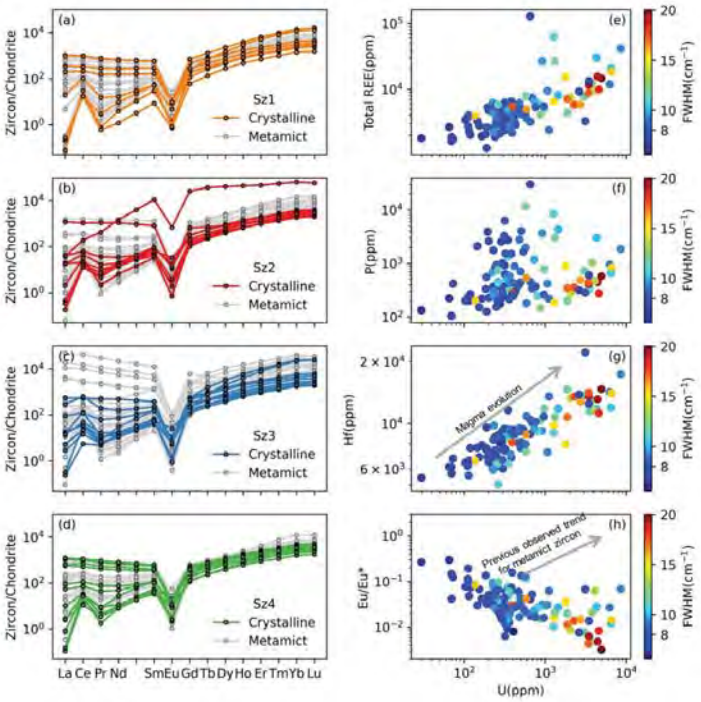

This is the peer-reviewed, final accepted version for American Mineralogist, published by the Mineralogical Society of America.
The published version is subject to change. Cite as Authors (Year) Title. American Mineralogist, in press.
DOI: https://doi.org/10.2138/am-2022-8075. http://www.minsocam.org/

Figure 6

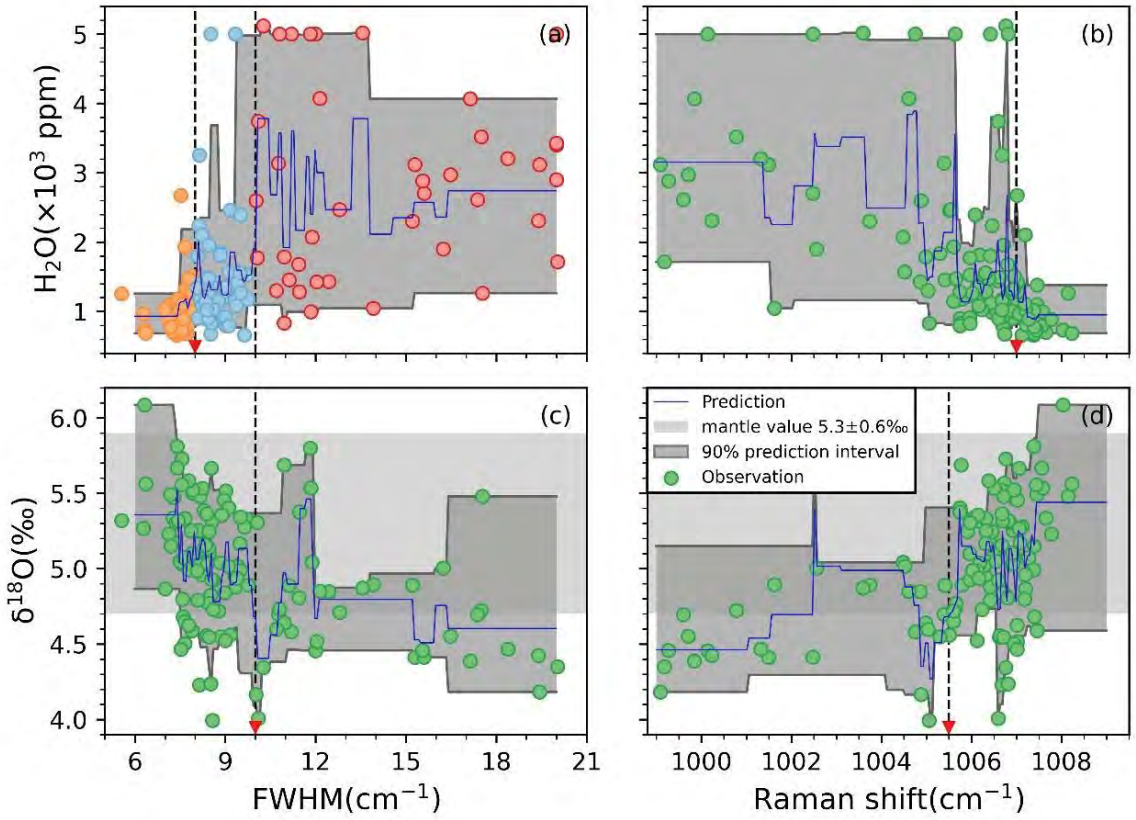

This is the peer-reviewed, final accepted version for American Mineralogist, published by the Mineralogical Society of America.
The published version is subject to change. Cite as Authors (Year) Title. American Mineralogist, in press.
DOI: https://doi.org/10.2138/am-2022-8075. http://www.minsocam.org/

Figure 7

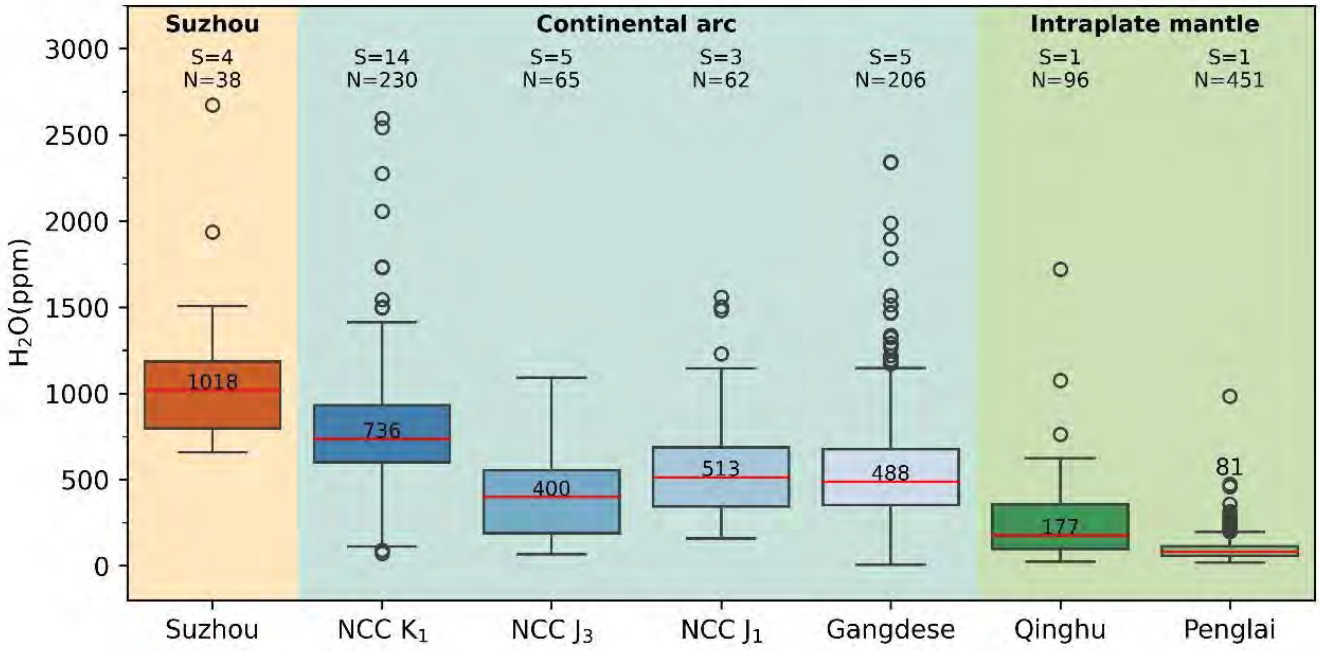

This is the peer-reviewed, final accepted version for American Mineralogist, published by the Mineralogical Society of America.
The published version is subject to change. Cite as Authors (Year) Title. American Mineralogist, in press.
DOI: https://doi.org/10.2138/am-2022-8075. http://www.minsocam.org/

Figure 8

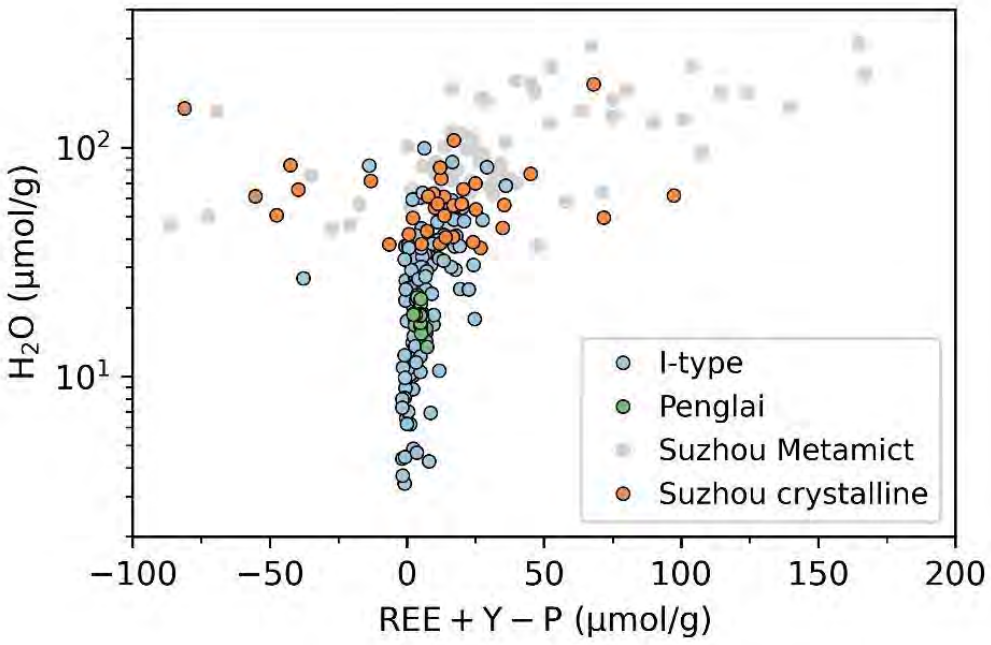

This is the peer-reviewed, final accepted version for American Mineralogist, published by the Mineralogical Society of America.
The published version is subject to change. Cite as Authors (Year) Title. American Mineralogist, in press.
DOI: https://doi.org/10.2138/am-2022-8075. http://www.minsocam.org/

Figure 6

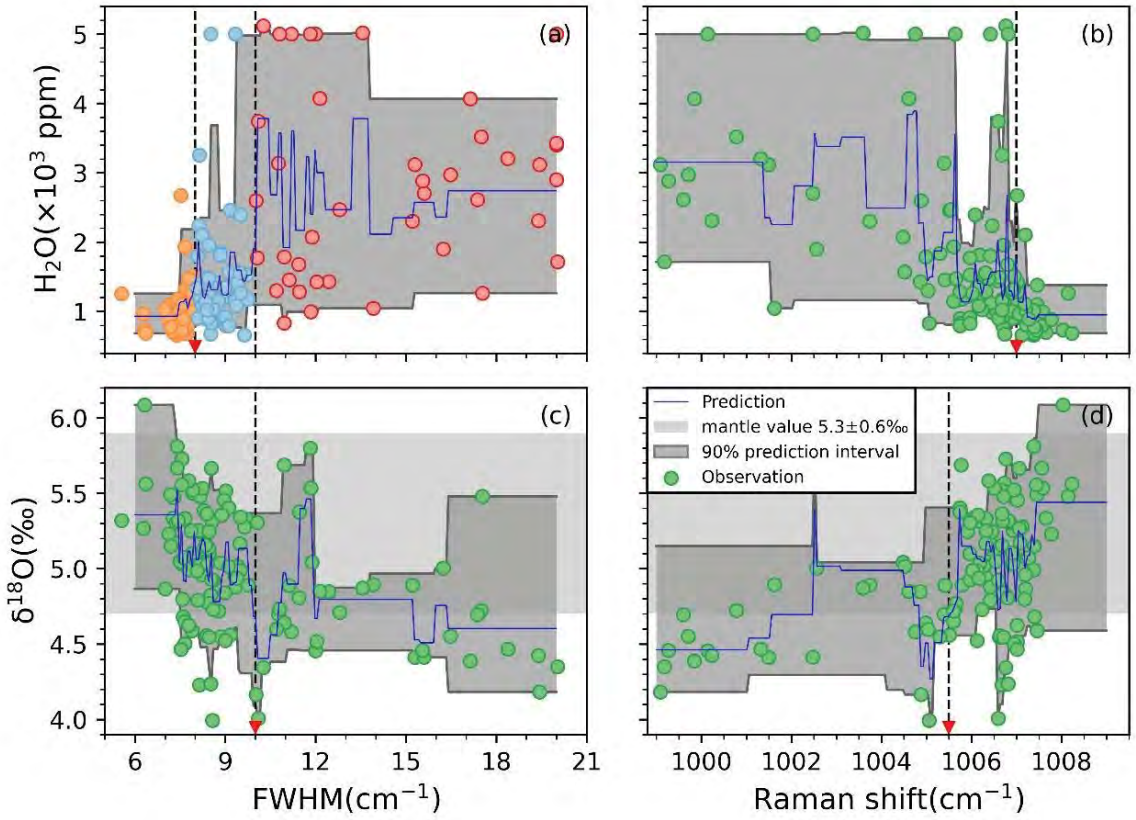

This is the peer-reviewed, final accepted version for American Mineralogist, published by the Mineralogical Society of America.
The published version is subject to change. Cite as Authors (Year) Title. American Mineralogist, in press.
DOI: https://doi.org/10.2138/am-2022-8075. http://www.minsocam.org/

Figure 7

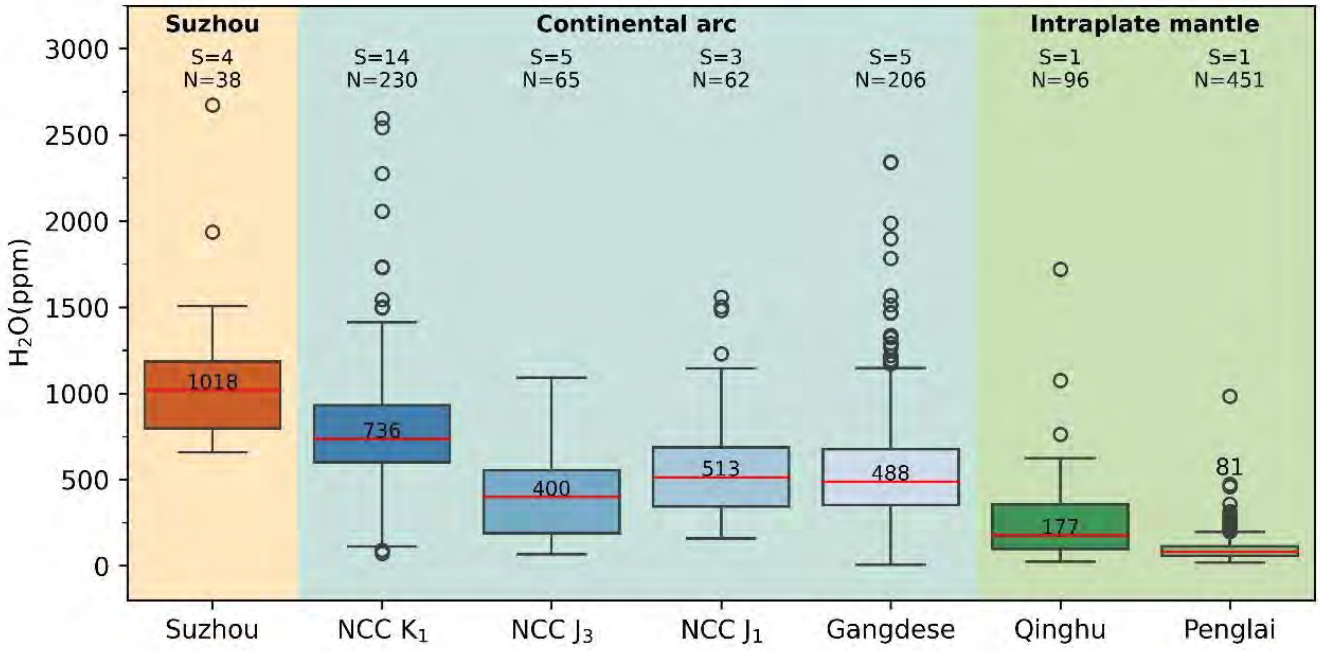

This is the peer-reviewed, final accepted version for American Mineralogist, published by the Mineralogical Society of America.
The published version is subject to change. Cite as Authors (Year) Title. American Mineralogist, in press.
DOI: https://doi.org/10.2138/am-2022-8075. http://www.minsocam.org/

Figure 8

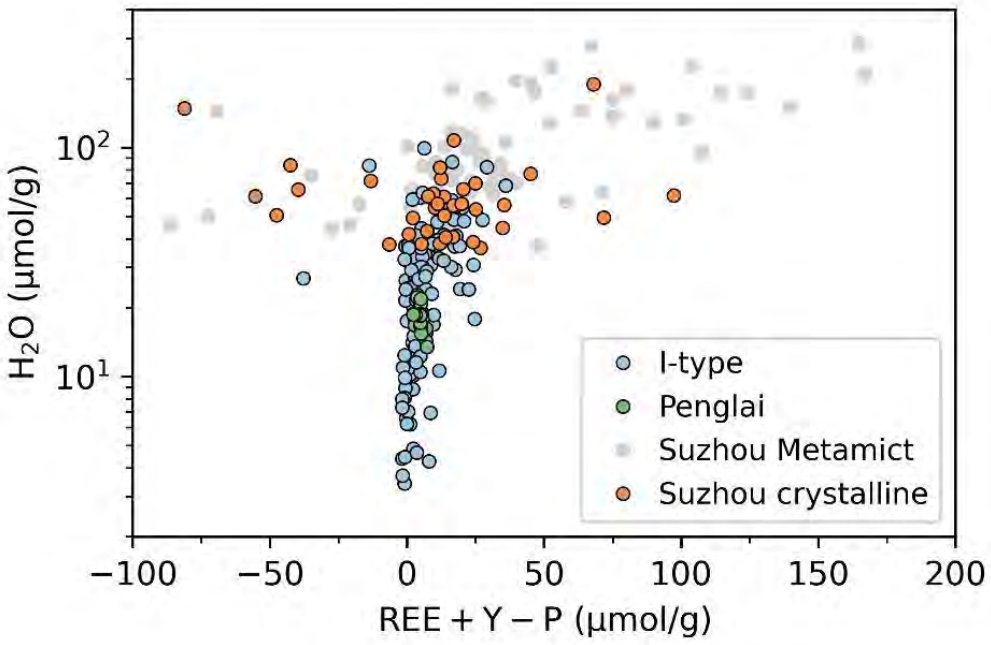

This is the peer-reviewed, final accepted version for American Mineralogist, published by the Mineralogical Society of America.
The published version is subject to change. Cite as Authors (Year) Title. American Mineralogist, in press.
DOI: https://doi.org/10.2138/am-2022-8075. http://www.minsocam.org/

Figure 7

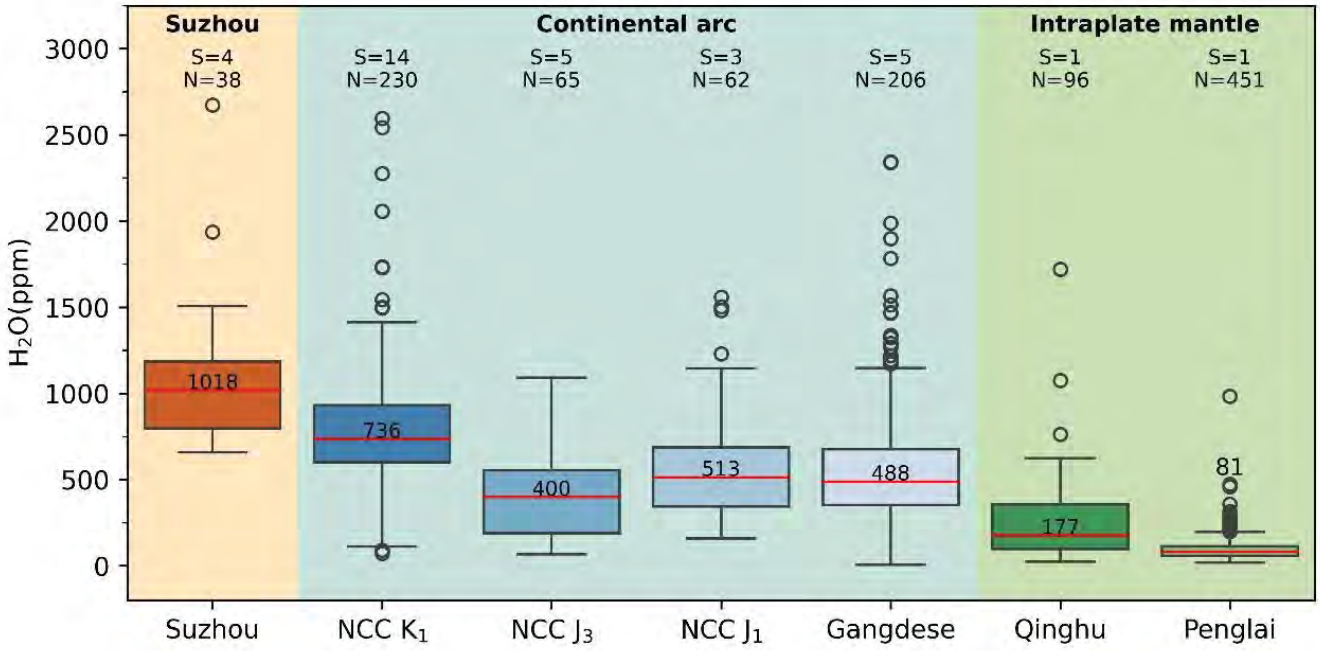

This is the peer-reviewed, final accepted version for American Mineralogist, published by the Mineralogical Society of America.
The published version is subject to change. Cite as Authors (Year) Title. American Mineralogist, in press.
DOI: https://doi.org/10.2138/am-2022-8075. http://www.minsocam.org/

Figure 8

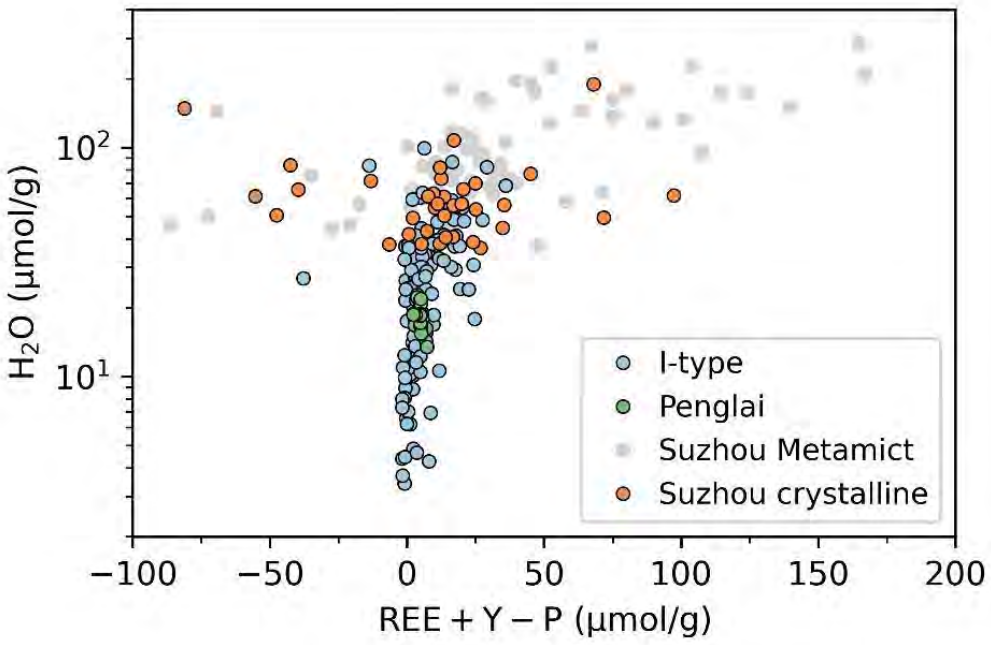

This is the peer-reviewed, final accepted version for American Mineralogist, published by the Mineralogical Society of America.
The published version is subject to change. Cite as Authors (Year) Title. American Mineralogist, in press.
DOI: https://doi.org/10.2138/am-2022-8075. http://www.minsocam.org/

Figure 8